TERAHERTZ (>0.3THz) ACTIVE IMAGING SYSTEMS

A THESIS SUBMITTED TO
THE GRADUATE SCHOOL OF NATURAL AND APPLIED SCIENCES
OF
MIDDLE EAST TECHNICAL UNIVERSITY

BY

FIRAT İDİKUT

IN PARTIAL FULFILLMENT OF THE REQUIREMENTS
FOR
THE DEGREE OF MASTER OF SCIENCE
IN
PHYSICS

FEBRUARY 2016

Approval of the thesis:

TERAHERTZ (>0.3THz) ACTIVE IMAGING SYSTEMS

submitted by **FIRAT İDİKUT** in partial fulfillment of the requirements for the degree of **Master of Science in Physics Department, Middle East Technical University** by,

Prof. Dr. Gülbin Dural Ünver
Dean, Graduate School of **Natural and Applied Sciences** ______________

Prof. Dr. Mehmet T. Zeyrek
Head of Department, **Physics** ______________

Assoc. Prof. Dr. Hakan Altan
Supervisor, **Physics Department, METU** ______________

Examining Committee Members:

Prof. Dr. Bülent Akınoğlu
Physics Department,METU ______________

Assoc. Prof. Dr. Hakan Altan
Physics Department,METU ______________

Assoc. Prof. Dr. Alpan Bek
Physics Department,METU ______________

Assoc. Prof. Dr. Asaf Behzat Şahin
Electrical and Com. Eng. Dept., Yıldırım Beyazıt University ______________

Assoc. Prof. Dr. İlker Ü. Uzun Kaymak
Physics Department,METU ______________

Date: ______________

I hereby declare that all information in this document has been obtained and presented in accordance with academic rules and ethical conduct. I also declare that, as required by these rules and conduct, I have fully cited and referenced all material and results that are not original to this work.

Name, Last Name: FIRAT İDİKUT

Signature :

ABSTRACT

TERAHERTZ (>0.3THz) ACTIVE IMAGING SYSTEMS

İdikut, Fırat
M.S., Department of Physics
Supervisor : Assoc. Prof. Dr. Hakan Altan

February 2016, 53 pages

Imaging systems based on terahertz waves are becoming an integral part of commercial and military screening applications. In this thesis, the prototype of active scan THz imaging system was constructed for detection of concealed objects at standoff distance longer than $5m$. The system was mounted on a platform that can adjust in height, tilt and azimuthal angle. The methods of generation and detection of THz signal are based on Schottky diode rectifiers and Schottky diode mixers. The wavelength of the continuous wave (CW) source is 880μm and measured output power was $7mW$. The detector was Schottky diode based mixer and heterodyne detection method was used. The source and detector are constructed in a transceiver architecture using a directional coupler specially designed for this frequency. The leakage due to the directional coupler limited the dynamic range of the system to at most $20dB$. The optical design of the active scan THz imaging system is based on Confocal Gregorian Geometry (CGG). In this geometry, the main elliptical mirror and secondary parabolic mirror were manufactured by machining bulk aluminum. The final

optical system utilized 6 mirrors in total: a flat mirror to turn the beam, a short focal length parabolic reflector to collimate the beam, an XY scanning galvanometer mirrors assembly utilizing beryllium mirrors, and the main as well as secondary manufactured mirrors. Before testing the system, the output frequency of the source was determined by using dichroic filter, a metal mesh of patterned circular holes. The XY galvanometer mirror assembly allowed for imaging at $2 frames/s$ speed. The final constructed system allowed for imaging a $0.5m$ x $0.5m$ field of view with $1.5cm$ resolution at a standoff distance of about $6m$. By using the prototype, it was shown that obscured objects causing specular reflections was successfully detected from standoff distance. A metal stick, behind clothes and having $3cm$ thickness, was imaged.

Keywords: Terahertz Imaging, Confocal Gregorian Geometry, Standoff Imaging, Active Imaging

ÖZ

TERAHERTZ (>0.3THz) AKTİF GÖRÜNTÜLEME SİTEMİ

İdikut, Fırat
Yüksek Lisans, Fizik Bölümü
Tez Yöneticisi : Doç. Dr. Hakan Altan

Şubat 2016 , 53 sayfa

Terahertz dalga boyu temelli görüntüleme sistemleri ticari ve askeri uygulamaların ayrılmaz bir parçası haline gelmektedir. Bu tezde, 5 metreden daha uzak mesafede gizlenmiş objeleri tespit edebilmek için tasarlanmış olan THz dalga boylarında aktif tarama yapabilen bir prototip geliştirilmiştir. Geliştirilen sistemin bir platformun üzerine yerleştirilmesiyle yükseklik, eğim ve azimut açısı ayarlanabilmektedir. THz sinyalini üretmek ve tespit edebilmek için Schottky diyot temelli çarpan ve karıştırıcılar kullanılmıştır. Sürekli dalga(CW) üreten kaynağın dalga boyu 880μm ve çıkış gücü$7mW$ olarak ölçülmüştür. Kullanılan detektör Schottky diyot temelli çarpandır ve heterodin tespit yöntemi kullanılmıştır. Belirlenen frekans için tasarlanan yönlendirici bağlaştırıcı sayesinde, kaynak ve detektör alıcı-verici mimarisinde tasarlanmıştır. Yönlendirici bağlaştırıcıdan kaynaklanan sızıntı sistemin ölçüm hassasiyetini en çok $20dB$ ile sınırlandırmaktadır. THz aktif görüntüleme sisteminin optik tasarımı eş odaklı Gregoryen geometrisi(CGG) temeline dayanmaktadır. Bu geometride, ana eliptik ve ikincil parabol ayna dökme alüminyumun işlenmesiyle üretilmiştir. Optik

sistemin son halinde toplamda 6 ayna kullanılmıştır; ışın hüzmesini döndürmek için düz ayna, ışını paralelleştirmek için kullanılan kısa odaklı parabol ayna, XY tarama yapmak için berilyumdan yapılan galvanometrik ayna bileşenleri, ana ve ikincil üretilen aynalar. Sistemin testinden önce, kaynağın çıkış frekansı bir metal parçasının üzerine örgü deseninde açılan dairesel deliklerin yerleştirilmesiyle oluşturulan dikroik filtre kullanılarak tespit edilmiştir. XY galvanometrik ayna bileşenleri $2kare/s$ hızında görüntülemeye imkân sağlamaktadır. Son kurulan sistem yaklaşık $6m$ mesafeden $0.5m$ x $0.5m$'lik görüş alanında ve $1.5cm$ çözünürlükte görüntüleme yapabilmektedir. Bu prototip kullanılarak, düzgün yansıma yüzeyine sahip gizlenmiş objeler başarılı bir şekilde uzaktan tespit edilmiştir. Bir elbisenin arkasına yerleştirilen 3cm kalınlığındaki metal bir çubuk gözlemlenmiştir.

Anahtar Kelimeler: Terahertz Görüntüleme, Eş Odaklı Gregoryen Geometrisi, Uzaktan Görüntüleme, Aktif Görüntüleme

To my dear Family

ACKNOWLEDGMENTS

I am most thankful to my supervisor Assoc. Prof. Dr. Hakan Altan and Assoc. Prof. Dr. Asaf Behzat Şahin for their guidance during my study.

I am also grateful to colleagues in Terahertz laboratory; especially doctoral students Vedat Ali Özkan,İhsan Ozan Yıldırım and Taylan Takan for their great contributions to this study.

Finally, I would like to thank to my family for always encouraging me to finish my study and giving their support to my decisions in my life.

This work was supported by ASELSAN-Radar and Electronic Warfare Systems Business Sector (REHIS), and The Ministry of Science, Industry and Technology under grant number 0994STZ2011-2.

TABLE OF CONTENTS

LIST OF TABLES

TABLES

LIST OF FIGURES

FIGURES

LIST OF ABBREVIATIONS

THz	Terahertz (10^{12}Hz)
RF	Radio Frequency
EM	Electromagnetic
TE	Transverse Electric
Tx	Transmitter
Rx	Receiver
CW	Continues Wave
SHM	Sub Harmonic Mixer
PM	Pulse Modulation
SNR	Signal to Noise Ratio
THz-TDS	Terahertz Time Domain Spectrometer
DRO	Dielectric Resonator Oscillator
PDRO	Phase-locked Dielectric Resonator Oscillator
SMA	SubMiniature version A
TTL	Transistor Transistor Logic
UCA	User Controlled Attenuation
FOV	Field of View
PSF	Point Spread Function
MTF	Modulation Transfer Function
FWHM	Full Width at Half Maximum

CHAPTER 1

INTRODUCTION

People have always been interested in light for centuries. First Isaac Newton examined sunlight by designing a prism experiment. This experiment uses the refraction properties of the light in order to separate the sunlight into different colors. His observation shows that white light does not contain a single color. It is the combination of different colors. During the following decades, more observations were made about light. Scientists have discovered the regions of the electromagnetic spectrum of the light. All of these discovered regions have different properties and are named with regard to where they are used. These regions are shown in Figure 1.1.

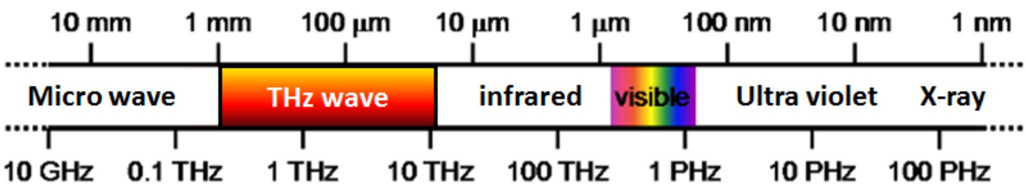

Figure 1.1: Electromagnetic Spectrum[1]

The generation of electromagnetic waves in the far infrared to radio region beyond the Microwave, which are mainly utilized for telecommunication and radar systems, can be done electronically or optically. These wavelengths are between sub-millimeters and meters. The transmitter and the receiver components are mainly based on the antenna technologies. In the other parts of the spectrum, the wavelength region is from sub-millimeter to nanometer. Region between infrared and microwaves are defined as the THz gap. Its range is defined from

$0.3THz$ to $10THz$. THz wave is called T-rays. In this range, T-rays have the optical properties as similar as the wavelengths where the light is modulated by using the optical components such as prisms, lens and polarizer. In THz gap, metal surfaces are used as a mirrors and some polymers based structures such as Polymethylpentene (TPX) and Teflon are mainly used as lenses. T-rays have also transmittance properties of the materials. In comparison to the infrared spectrum, T-rays penetrate into the organic structures as well as plastic, cloths and paper. The radiation of THz is non-ionizing, so it is harmless to living organisms and it does not destroy the molecular structure of the materials unlike X-rays [2].

T-rays have been a hot topic in 21th century due to their advantages in EM spectrum. It is sensitive to the polarity of the materials. In many research areas, the radiation interacts with the polar structures in material and this interaction gives the material to a fingerprint in THz region [3]. The most well-known technique which gives the fingerprint of the materials is THz Time Domain Spectroscopy (TDS). It uses THz pulses and scans the wide range of THz radiation on the sample, and measures the transmittance characteristic of the materials.

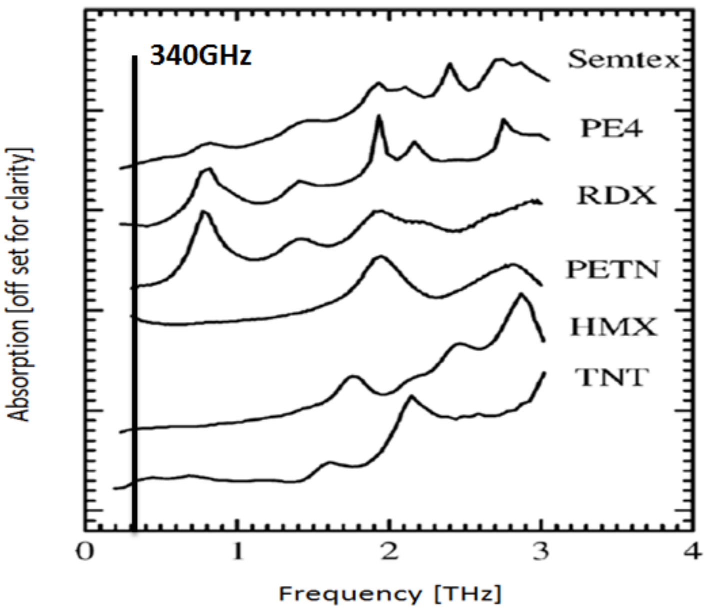

Figure 1.2: Absorption graph of explosives[2]

Today, one of the most studied areas of T-rays is in the area of security applications. Due to increase in terrorist and criminal actions in the last decades, scientists are trying to develop and improve the detection systems by using T-rays. It is observed that above 500GHz or so, some explosives and materials have fingerprint in THz domain. In figure 1.2, the fingerprints of the some explosives are shown [2]. The black line in figure 1.2, the source ($340GHz$) used in this thesis is not tunable. Therefore, the source cannot be used for finding the fingerprint of the explosives. It will be used for detection of a concealed object.

In addition to the explosive, T-rays are reflected from the metal surfaces. With the penetration of THz into the clothes, detection of the metal objects like guns and knife becomes possible.

Detection of the concealed objects is a very challenging issue in public areas such as airports, shopping centers and parks. Therefore a fast, effective and reliable measurement is needed using T-rays. To make an effective detection, THz passive and active imaging systems are being developed in the last decades. These systems will be described in the next sections.

In these areas, T-rays will travel into the air medium. The rate of humidity of air creates an absorptive medium in THz region. However, there are special windows that the transmittance of T-rays is very efficient [4].

In Figure 1.3, the transmittance spectrum of THz gap with respect to the relative humidity level is shown. The windows are in $0.3 - 0.55THz$, $0.55 - 0.75THz$, $0.75 - 1THz$ and so on. In this thesis, THz source are designed into the window having transmittance between $0.3 - 0.55THz$.

1.1 THz PASSIVE IMAGING SYSTEMS

The passive imaging systems detect objects by using the thermal radiation difference between the object and background. Every material emits EM radiation which is called black body radiation [5]. The radiation energy of the materials depends on the temperature of the material.For example, the energy of

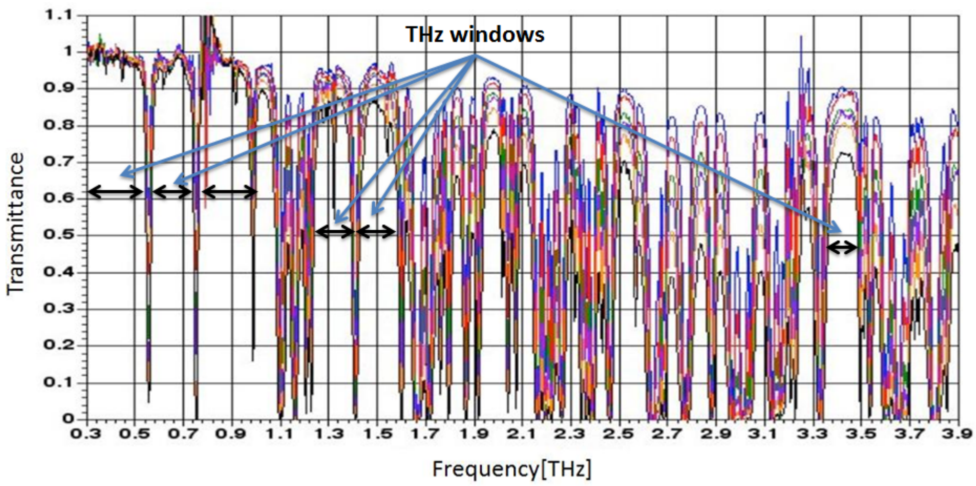

Figure 1.3: Tranmittance windows of THz in air. (Blue, red, green, purple, orange, and black lines correspond to 6%, 12%,22%, 26%, 40%, and 52% relative humidity, respectively) [4]

T-rays($1THz$) is $4.1meV$ at $300K$ [6]. In THz passive imaging systems, the black body radiation is used for THz source. Because it is produced by materials, it is not a coherent radiation such as electronic THz sources or lasers. The incoming radiation is typically collected by optics and coupled into detector [5]. The quality of the image is related to the signal to noise ratio(S/N) of the system. The bigger (S/N) ratio is achieved, the better image quality is obtained.

$$S/R = \left(\frac{T_I}{T_N}\right)\left(\frac{b}{B}\right)^{\frac{1}{2}} \tag{1.1}$$

In equation above, S/N definition is given in which b is the optical bandwidth (IF) of the system,B is bandwidth with the integration time, T_I is the temperature of thermal source, and T_N is the noise temperature of the receiver. In general, although the passive systems do not have the large dynamic range as compared to the active systems, they are basically multimode and this compensates the smaller dynamic range of the system[5].

1.2 THz ACTIVE IMAGING SYSTEMS

Instead of detecting THz radiation of the object, it is illuminated by coherent T-rays source. Beause of using THz source, illumination of the objects increases the dynamic range of the system. In active systems one can also modulate the generated signal which can be pulse or continuous wave (CW). The pulse modulation can provide the distance information of the objects. The time travel of the pulse and the duration of the pulse effect the resolution of the distance. More detailed explanations will be given in chapter 3. In CW mode, the object is illuminated by a focusing system and the reflected beam from the target is coupled into the receiver[7]. This system consists of the two parts which are transmitter and the receiver. It is also possible to use the same optical geometry, used on the passive imaging system, in active imaging system[5].

1.3 RADAR POWER CALCULATIONS

In this thesis, the received power of 340GHz system mainly affects the performance of the scanning system. In radar technology, the transmission of the power from the transmitter to the receiver antenna throughout the medium has an important role of radar technologies such as GPS, cellular phones, antennas. To calculate the received power of the antenna, the Friis Transmission equation is used. The compact form of the equation is shown in equation 1.2[8].

$$P_r = \frac{P_t G_t G_r \sigma F^4}{(4\pi)^2 R^4} \tag{1.2}$$

The dominant term of the equation is the distance between the transmitter and the receiver. This equation states that the transmitter is a point source and emits the radiation to the space. Therefore, the received power is proportional to $1/R^4$ of the distance. However, active scanning systems are designed in transmission geometry, so the total power of the source is transferred to the area or target. In figure 1.4,the transmitter power decreases with respect to $1/R^2$ for standoff detection with the isotropic scattering assumption of the scattering target as discussed by Brown[9].

$$P_r = A_r \left(\frac{P_t}{\Theta(2D)^2} \right) e^{-2\alpha_b L_b} e^{-2\alpha_a D} e^{-2\alpha_e L_e} \tag{1.3}$$

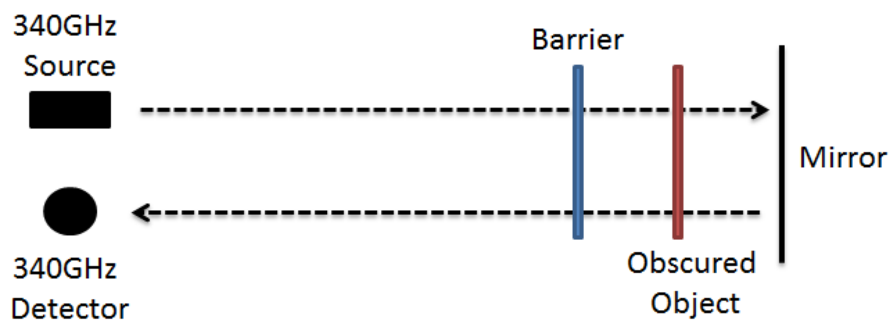

Figure 1.4: Transmittance geometry for detection of the hidden object [10]

In equation 1.3 [10],A_r is the area of the receiver,P_t is the transmitted power, Θ is the solid angle of the directed transmitted power,L coefficients are the thicknesses of the barrier and the explosives,D is the distance of the target, and α_a,α_b,α_c are the absorption coefficient of the free space, barrier and the obscured object. In chapter 4, the received power of the system coming from the flat metal surface will be calculated by using equation 1.3.

In this thesis, 340GHz active imaging systems is designed by using Schottky diode based rectifiers and mixers. The heterodyne detection methods based on Schottky diode mixers, XY-galvo scanning mirrors are used to obtain standoff imaging by designing Confocal Gregorian geometry [11]. In the second chapter, the generation and the detection methods of CW THz radiation will be introduced. In the following chapter, the architectural design of 340GHz heterodyne source and the characterization of the systems will be discussed. In the fourth chapter, the optical design, Confocal Gregorian geometry, and the performance of the design will be discussed. In the final chapter, the thesis will be concluded with a summary.

CHAPTER 2

GENERATION AND DETECTION OF THZ RADIATION

THz radiation can be generated in many ways. For example, mercury arc lamps, optically pumped gas lasers, photoconductive antennas, photomixers[12], UTC-PD (uni-travelling-carrier photodiode)[13], YIG (Yttrium Iron Garnet) oscillators, DROs, and Schottky diode multiplier structures are the some of the possible generation methods. In this thesis, the DRO oscillators are used for the main THz generation. In order to obtain THz radiation $[0.3 - 1THz]$ by using these sources, Schottky diode based multipliers and the mixer are assembled in cascade form to radiate THz wave. In this chapter, RF components that are used for generating THz and the some detection methods of THz radiation will be studied to provide background to the 340 GHz transceiver system.

2.1 GENERATION

2.1.1 DRO and PDRO Sources

DRO was first illustrated by R.D.Richtmyer in 1939 [14]. In principle, a long cylinder of dielectric material can serve as a resonator for electromagnetic waves of certain frequencies. It has been investigated using various shapes of design circuits during the last three decades[15]. It is a low cost microwave signal generator having a small size, low-phase noise ratio, high-Q-factor and frequency stability. The frequency stability property of this device extends the application areas such as measuring the properties of antennas[16], filters [17] and the oscillators[18].

In case of the compactness, the resonator is mainly made of the materials having the high dielectric constants ($\epsilon_r > 35$). In addition to that, the resonator cavity is enclosed to preserve the temperature stability of the oscillator and the high Q factor.

For the simplicity of the design, the dielectric material having cylindrical shape is preferred. The shape has some advantages. First, it provides easy separation between the TE_{01} mode and the other higher order modes. Second, it is easy to couple the resonant frequency to the micro strip circuit. The last one, it is easy to mount.

In this thesis, PDRO frequency generator is used for the reference source. PDRO contains a feedback controlled circuit. The feedback circuit has the crystal oscillator to improve frequency stability and phase noise on the tuned voltage controlled oscillator (VCO). PDRO has extremely better phase noise performance and frequency stability than DRO. However, the frequency stability of phase-locked DRO causes the variation in output power, while tuning the DRO [19]. In this study, $340GHz$ source will be operated in CW and pulse modulation at $340GHz$, so the output power will be affected by the type of modulation. In chapter 3, the system will be explained in detail.

2.1.2 Diode Frequency Multipliers

The main component of the generation of THz radiation is the diode frequency multiplier (schottky diode). The generated signal of DRO is up converted to the THz range by schottky diode. In this part, the working principle of the schottky diode and frequency conversion operations will be discussed.

Schottky diode is one of the most important tools for detection of the Radio Frequencies (RFs) because it is used for both switching due to the natural behaviour of the diode, and a frequency multiplier. Schottky diode is a semiconductor device. It is made of metal and semiconductor connection.

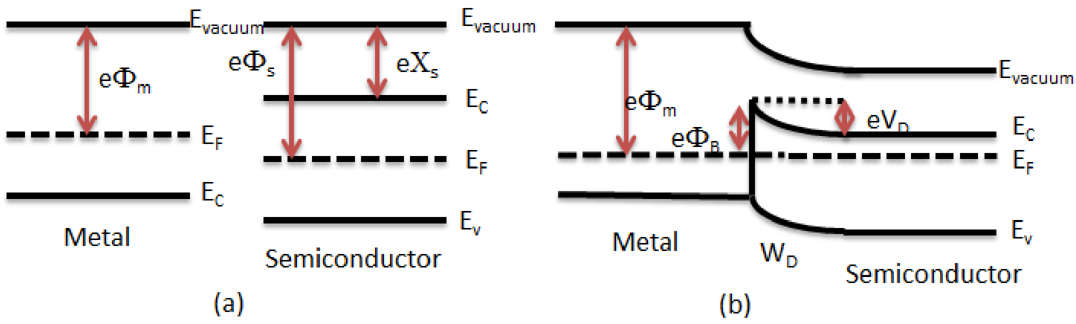

Figure 2.1: (a)Band diagram for metal and semiconductor,(b) Metal and semiconductor in contact under the equilibrium (fermi level). $e\Phi_m$ and $e\Phi_s$ are work function of metal and semiconductor. $e\chi_s$ is electron affinity of semiconductor. E_{vacuum}, E_C, E_F and E_V are vacuum level,conduction band level,Fermi level and valence band level. [20]

In figure 2.1(a), it shows us the energy band diagram of the metal and semiconductor materials before the connection of two materials. After the connection the energy band diagram of the materials is indicated in figure 2.1(b).

In figure 2.1(b), it is observed that the conduction band level E_c of the semiconductor is decreasing due to the electron flows through the metal until the Fermi levels E_f became equal. This is called the zero bias condition. After the electron flows, it is observed a decay of conduction band level which creates a potential barrier having magnitude $e\Phi_B$ and a depletion width W_D. This barrier is called by Schottky barrier. V_D is the diffusion potential and it can be defined by the equation 2.1.

$$eV_D = e\Phi_B - (E_c - E_f) \tag{2.1}$$

The Schottky diode is a nonlinear device and the nonlinear voltage-current characteristic of the diode is shown in figure 2.2(c). When the input sinusoidal signal is applied on diode, the nonlinearity property of the diode will cause the generation of the harmonics with a carrier frequency which is the integer multiple of the input frequency. In figure 2.2(b), the output frequency and its' harmonics are shown in frequency domain. After the multiplication process, the undesired harmonics are eliminated by the filters.

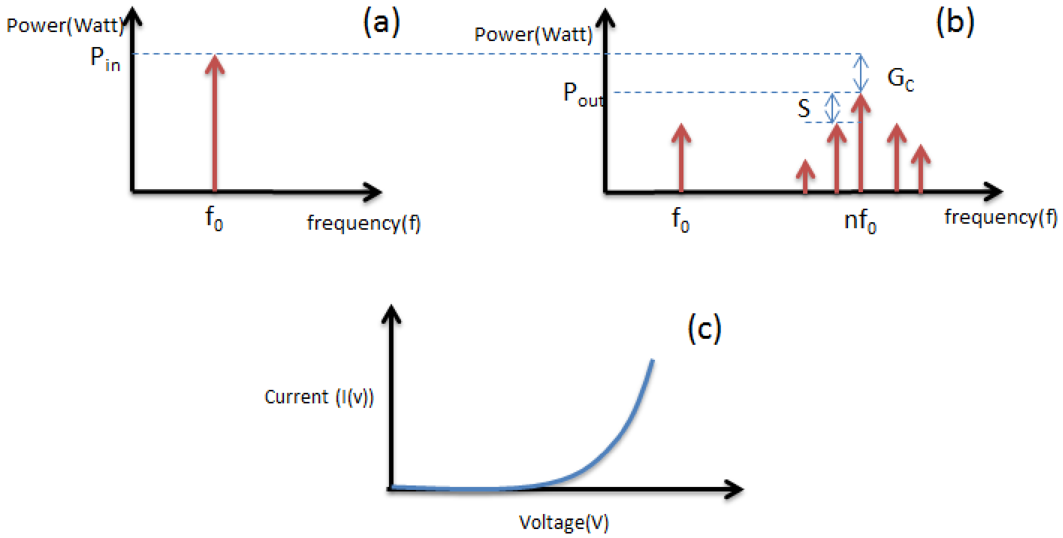

Figure 2.2: (a)The input frequency f_0 having P_{in} input power (b) the output frequency nf_0 having P_{out} output power with its harmonics,where n is the multiplication factor, G_C is the conversion gain and S is the suppression of undesired harmonics. (c) The nonlinear voltage-current graph of schottky diode[21]

2.2 DETECTION

2.2.1 Schottky Diode Heterodyne Detection

In this type of detection, there are local oscillator(2.3) and received signal (2.2) with different frequencies generated by two sources. These two waves are mixed in the sub-harmonic mixer (SHM). In RF measurements, a mixer is an important device. It performs the multiplication of the two signals and by doing so, the signal is carried at higher or lower frequency levels. Schottky diode based SHM performs the multiplication process. In figure 2.3, the flow graph of the mixer is shown.

In order to make this concept clear, mathematical representation of mixer can be useful.

$$\Psi_{RF} = |A_{RF}| cos(2\pi f_{RF} t + \phi) \tag{2.2}$$

$$\Psi_{LO} = |A_{LO}| cos(2\pi f_{LO} t) \tag{2.3}$$

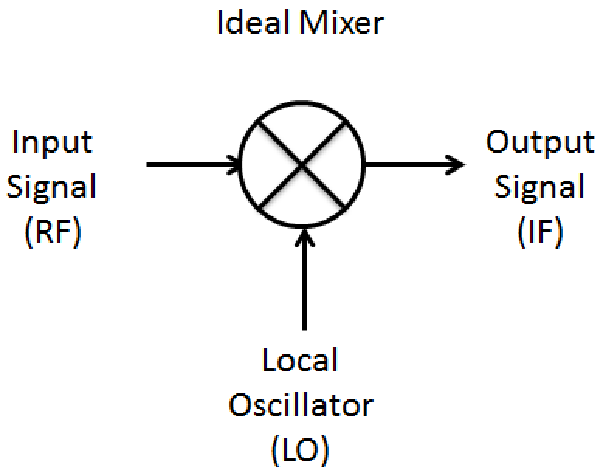

Figure 2.3: The ideal mixer flow graph

$$\Psi_{RF}\Psi_{LO} = |A_{RF}|cos(2\pi f_{RF}t + \phi)|A_{LO}|cos(2\pi f_{LO}t) \tag{2.4}$$

$$= \frac{1}{2}|A_{RF}||A_{LO}|[cos(2\pi(f_{RF} + f_{LO})t + \phi) + cos(2\pi(f_{RF} - f_{LO})t + \phi)] \tag{2.5}$$

After the multiplication of the two signals having the frequencies f_{RF} and f_{LO}, two cosine terms are obtained. However, only the one of the component is survived which is $cos(2\pi(f_{RF} - f_{LO})t + \phi)$ term.The higher frequency component is eliminated by filtering. The intermediate frequency (IF) component can be obtained by this multiplication. IF contains the information about the transmitted signal such as intensity, the type of modulation and the phase. In addition to the information obtained by IF signal, the signal is in megahertz range which means that IF signal can be measured by the low cost electronic devices such as oscilloscope, DAQ card and so. IF frequency is defined the equation below.

$$f_{IF} = f_{RF} - f_{LO} \tag{2.6}$$

In addition to mixing operation, the intensity of received signal is derived by the following relations;

$$I \approx (\Psi_{RF} + \Psi_{LO})^2 \tag{2.7}$$

$$I = |A_{RF}||A_{LO}|cos(2\pi(f_{RF} + f_{LO})t + \phi) + |A_{RF}||A_{LO}|cos(2\pi(f_{RF} - f_{LO})t + \phi)$$
$$+ \frac{|A_{RF}|^2}{2}(1 + cos(2\pi f_{RF}t + \phi)) + \frac{|A_{LO}|^2}{2}(1 + cos(2\pi f_{RF}t)) \quad (2.8)$$

$$I = \frac{|A_{RF}|^2 + |A_{LO}|^2}{2} + |A_{RF}||A_{LO}|cos(2\pi(f_{RF} - f_{LO})t + \phi) + \frac{|A_{RF}|^2}{2}cos(2\pi f_{RF}t + \phi)$$
$$+ \frac{|A_{LO}|^2}{2}cos(2\pi f_{RF}t) + |A_{RF}||A_{LO}|cos(2\pi(f_{RF} + f_{LO})t + \phi) \quad (2.9)$$

The high frequency components $(2f)$ are eliminated by filtering. The remaining constant and the beat components can be provide us the intensity. It is also possible to obtain the phase information. In addition to that, this technique has good signal to noise ratio.

2.2.2 Schottky Diode Homodyne Detection

In this detection, output signal is separated by using the interferometer and the small amount of the signal is used as local oscillator. Because of this the receivedRF and the LO signal have common frequency. To calculate the intensity of the detection equation 2.7 can be used. However in this case, f_{RF} is replaced by f_{LO}. By eliminating higher orders terms of the equation 2.8 will give the result:

$$I \approx \frac{|A_{RF}|^2 + |A_{LO}|^2}{2} + |A_{RF}||A_{LO}|cos(\phi) \quad (2.10)$$

In equation 2.9, ${E_{LO}}^2$ term is negligibly small compared to the other terms. Therefore, it can be eliminated. In addition, the phase information still survives. However, the drawback of this system is that it is hard to align.

2.2.3 Golay Cell

It is a widely known detector which is invented in 1947 by M.J.E Golay [22]. It is operated at room temperature. The block diagram of the detector is shown in figure 2.4.

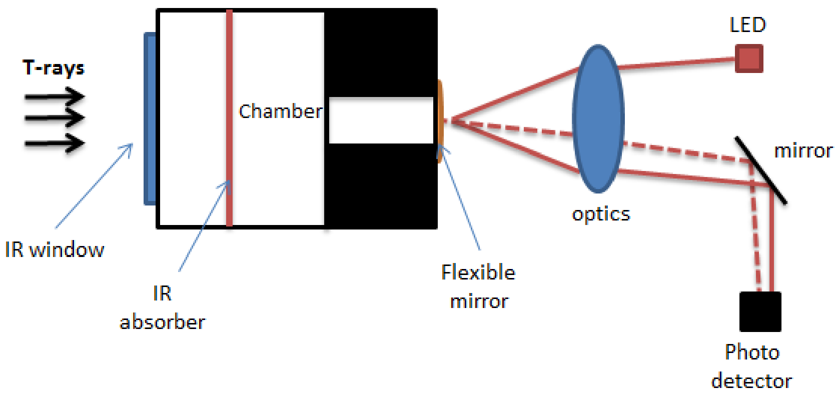

Figure 2.4: The block diagram of Golay Cell [23]

In principle, the incoming radiation is passed through IR window. After that, the radiation falls on the IR absorber, a thin metal film. The absorbing film transfers the heat generated from the radiation to the chamber which is filled with a small volume of the gas (Xenon). The increase in the temperature of the gas causes the thermal expansion, so the pressure increases[23]. The chamber is connected to a flexible mirror. Changing the pressure of chamber results the vibration of the mirror. The vibration of the mirror is detected by the photoacoustic methods [24]. The LED illuminates the mirror and the vibration of the mirror changes the coupled intensity of the photo detector. The performance of the Golay Cell depends on time needed to change the pressure of the gas under the modulation of the incoming radiation. It is a thermal detector and there is a relaxation time of the gas leads to decreasing the pressure. Therefore, the readout circuit of the photodetector is designed as AC coupled [22]. The measured power depends on the speed of the modulation. It has an modulation frequency range between $5Hz$ and $70Hz$. However, the responsivity of the measured power changes in different frequencies. In figure 2.5, the responsivity curve of the Golay Cell which is used in our laboratory is shown. In chapter 3, the measurements made by Golay Cell will be discussed.

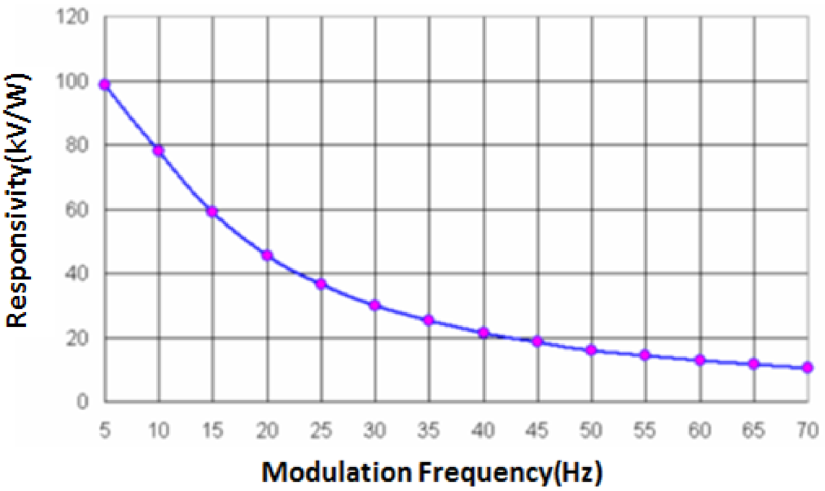

Figure 2.5: The responsivity curve of the Golay Cell (Tydex GC-1P)

CHAPTER 3

340GHz CW TRANCEIVER SYSTEM AND ITS' CHARACTERIZATION

3.1 340GHz SYSTEM CONFIGURATION

$340GHz$ millimeter wave system is divided into two parts which are the transmitter (T_x) and the receiver (R_x). The block diagram of this system is shown in figure 3.1. The combination of these two parts with one common antenna is called transceiver system. In table 1, the components of $340GHz$ system are listed. The first components of these two parts are the $10MHz$ crystal oscillators. After the oscillators, an RF coupler in receiver and the RF switch in transmitter are connected between the external reference output and the external reference input by SMA cables in order to synchronize the phases of the crystal oscillators. Making the phase measurements or stabilizing the temperature dependent frequency shifts due to the surrounding medium or cavity, it is important to turn the RF switch on between these oscillators. However, if the system is running in the room, the stable room temperature does not affect the system performance because the rest of the components are attached to the metal surface or fan coolers.

As frequency sources, the same PDROs are used in both parts of the system. The central frequencies of these PDROs are fixed at 14.2GHz in receive and 14.18GHz in transmitter. The output power of both is around $15dBm$. The SMA cables are used for connecting the PDROs to the RF couplers.

The system contains a TTL modulation switch on the voltage box (17^{th} component). The signal can be modulated with DC-20GHz pin-switch having $1ns$ rise time. Under the forward bias, this switch behaves like resistor and also under the reverse bias it runs like a capacitor. By applying the bias on PIN switch structure and changing the impedance of the switch the wave can be modulated [25]. By using the switch TTL pulse modulation is generated and the measurements have been recorded. In the measurement part, this will be explained more clearly.

Each PDRO has RF coupler output port. By making connection between RF output port and spectrum analyzer, the generated signal is observed and it makes sure that the temperature dependent frequency shifts have been stabilized. By this way, the generated PDRO signal of both T_x and R_x part are controlled.

3^{th} component of the system is the passive signal amplifier. It has high gain medium and it amplifies the signal power up to $24dBm$. The connections are again made by SMA cable.

5^{th} elements of the system are the Virginia Diodes Incorporated (VDI) voltage boxes. Both T_x and R_x parts have their own voltage control box. The boxes are connected to the shottky diode multipliers. These boxes provide the user with controlling the output power of the source and the modulation of the waveform which has alternative shapes such as sinusoidal, rectangle and square shapes. For example, the output power is measured by Golay Cell which requires modulation on itself or the source in order to eliminate background radiation and obtain AC output. In order to make the measurement, TTL or UCA external inputs on T_x voltage box is connected to the waveform generator by BNC cable. The square wave is already defined on waveform generator having external TTL output. UCA modulation is operated on channel outputs of the generator. The amplitude, frequency and waveform are specified by UCA modulation.

The next elements of the system are 4^{th} , 6^{th} and 7^{th} which are the schottky diode multipliers. In the receiver part, the multipliers are placed in an order of $x2x2x3$. The 4^{th} component multiplies the signal to the 28.4GHz. After that multiplication, SMA cables reaches the limits in order to transfer RF signal to the next multipliers, so the next components are connected as the waveguide cascade structure [26]. The receiver signal is used for mixing with the returning signal and it is not needed to generate high power signal, so the bias voltages is only applied on $x2x2$ components by SMA cables. After the multiplication of the oscillator signal ($14.2GHz$), the signal is up converted to $170.4GHz$.

In transmitter, the multipliers are placed in an order of $x3x2x2x2$. In this part, the bias voltages are applied on all schottky diodes by SMA connections. After the multiplications, THz wave is generated. The total order of multiplication is $3x2x2x2 = 24$. The output frequency of the transmitter is obtained from the multiplication of the PDRO with the order $x24$ is $340.32GHz$.

9^{th} element of the system is the directional coupler. It connects the transmitter and the receiver to a common horn. The returning signal coming from the target is coupled to the horn again. This coupler provides transmitter part with $30dB$ isolation to protect the multipliers from burning and transfer the incoming signal to the sub-harmonic mixer (8^{th} element).

The 8^{th} component is the sub-harmonic mixer(SHM). In this component, the signal generated ($170.4GHz$) in receiver is doubled ($340.8GHz$) and the returning signal from the target is mixed with $340.8GHz$. In this process, the two frequencies are generated. The mixing process is simply explained in equation 3.1.

$$2cos(R_x)Cos(T_x) = cos(T_x - R_x) + cos(T_x + R_x) \tag{3.1}$$

It explains that the two frequencies which are defined as high frequency and the low frequency components. The high frequency component ($T_x + R_x$) is eliminated by low pass filter in SHM and the low frequency ($|T_x - R_x| = IF$) component survives. Obtaining the IF component by mixing two high frequency signals is named down sampling[27]. The IF is the order of MHz range and this provides observing the signal with electronic devices such as spectrum analyzers, oscilloscope and DAQ card.

11^{th} component is the amplifier. It amplifies the IF signal before it is connected to the measurement instruments. The power measurements and the verification of the output signal will be discussed in the next parts of chapter 3.

Table3.1: System Components

Component number	Components
1	10MHz Crystal Oscillators (reference oscillator)
2	14.18GHz (Tx)/14.2GHz (Rx) PDRO
3	Amplifier (24dB Gain, 6-18GHz)
4	x2 (25-31GHz Spacek Labs A286 HP Doubler)
5	VDI Voltage Bias Box
6	x2 (50-70GHz VDI WR15x2 Doubler)
7	x3 (140-220 GHz VDI WR5.1x3 Tripler)
8	SHM (260-400 GHz Sub-Harmonic Mixer WR2.8SHM)
9	High Directivity Coupler – WR2.8 (3dB)-VDI
10	RF Waveguide Coupler (6-18GHz)
11	Amplifier (15dB gain, 50MHz-6GHz)
12	x3 (37.5-42.5GHz Spacek Labs A415 HP Tripler)
13	x2 (60-90GHz VDI D84 Narrowband Doubler)
14	x2 (120-180GHz VDI D175 Narrowband Doubler)
15	x2 (240-360GHz VDI D320 Narrowband Doubler)
16	WR2.8 Pyramid Horn
17	DC-20GHz 1ns PIN SWITCH (AMC SWM-DJV-1DT-2ATT)

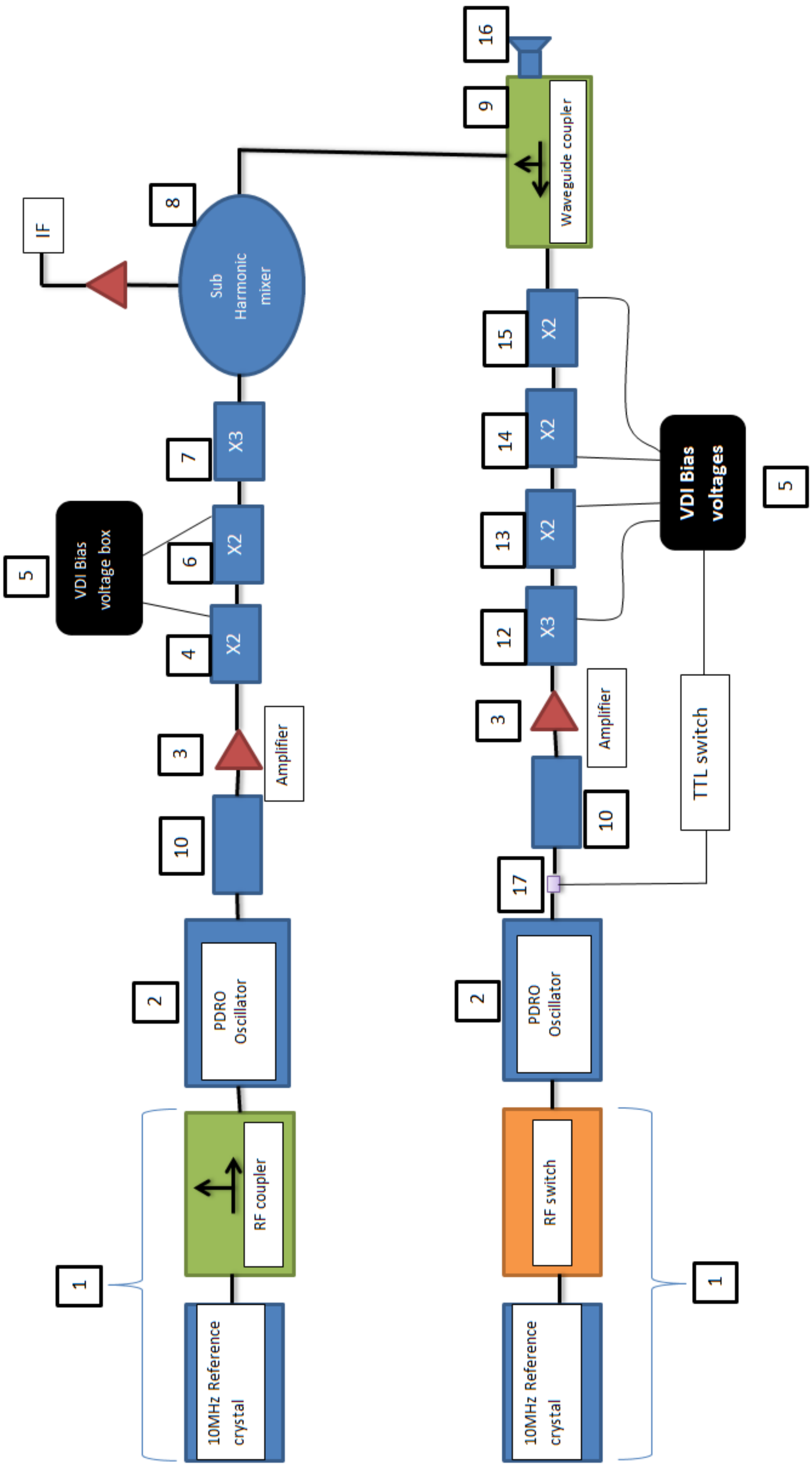

Figure 3.1: The block diagram of 340GHz system

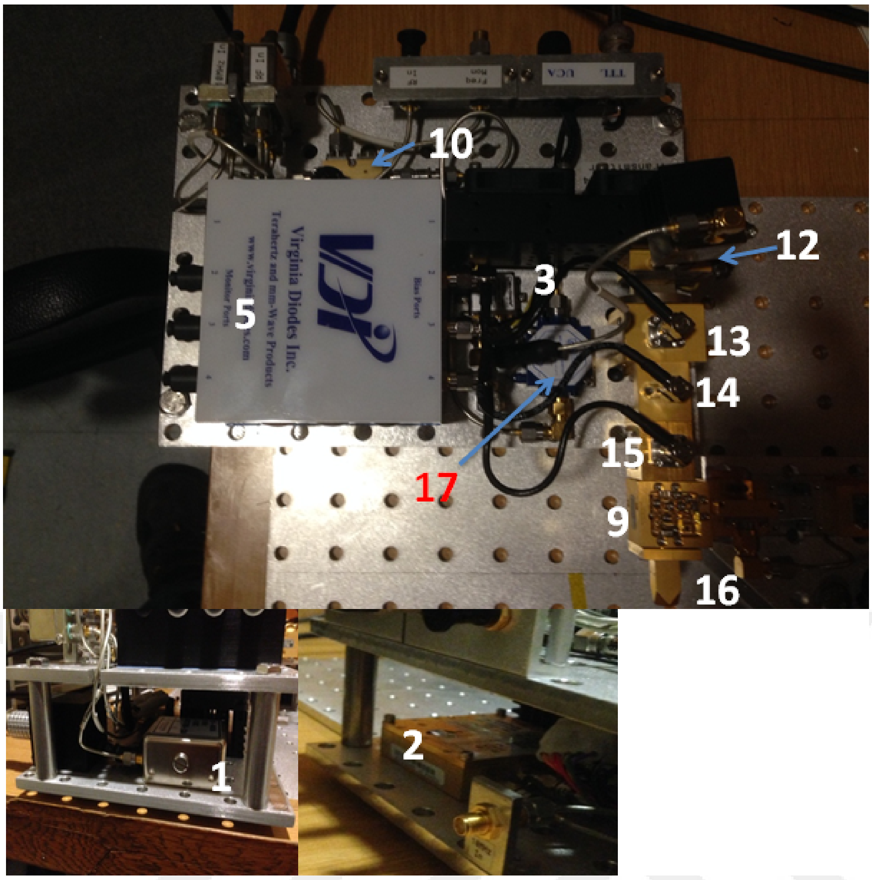

Figure 3.2: The transmitter picture and its' components

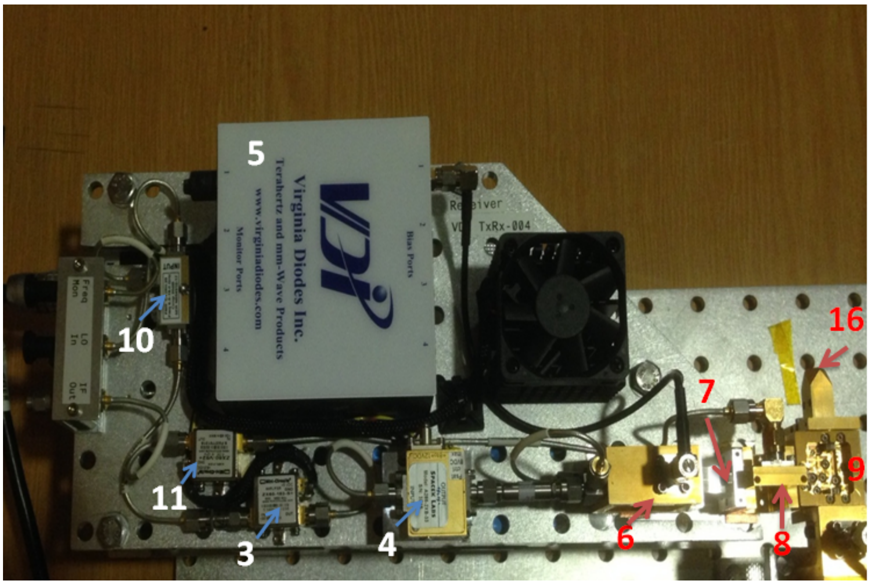

Figure 3.3: The receiver picture and its' components

3.2 IF MEASUREMENT

In figure 3.4, the first spectrum measurement of the IF signal and the harmonics are observed by Marconi 2383 spectrum analyzer. The analyzer was set to $1MHz/div$ horizontally and $10dBm/div$ vertically. The source was modulated by the square wave ($1MHz$) to observe the harmonics of the waveform into the IF spectrum. At the center of the figure, the dashed lines are locked to the IF signal, having $0.475GHz$ frequency with $-7.5dBm$ power. The first harmonics of the modulation is on $0.476GHz$ and $0.474GHz$. The power deviation between IF and its' harmonics are -5, -20 and $-40dBm$. This means that the harmonics are quite small with respect to IF signal.

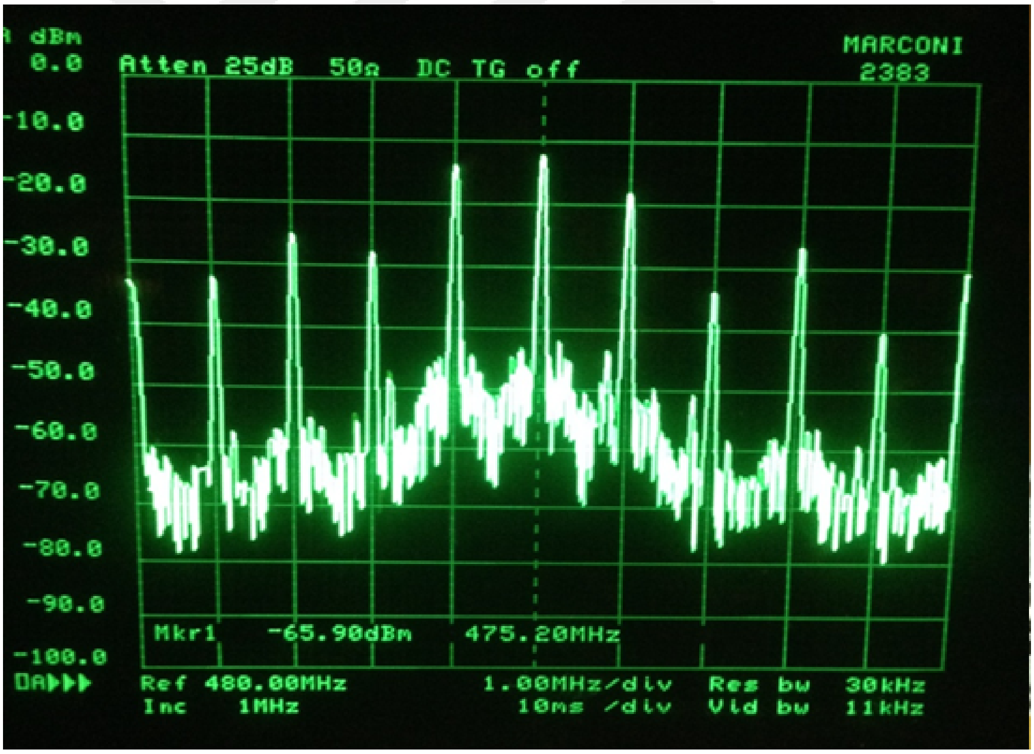

Figure 3.4: IF signal with the harmonics of square modulation at 1MHz measured by Marconi 2383 spectrum analyzer

3.3 OUTPUT POWER AND THE GAUSSIAN BEAM PROFILE MEASUREMENT

The output power of the transceiver system was measured by the Golay Cell (Tydex GC-1P) in laboratory. This device has the operating wavelength range between 15μm and 8000μm. The responsivity of the Golay Cell changes from microwatt to miliwatt. The measurement is made in volt units and the responsivity curve given by the Golay Cell is used to convert the measured voltage into the watt. The responsivity Curve is shown in figure 2.5.

In order to measure the total output power and confirm the Gaussian beam profile of 340GHz source, an experimental setup was prepared.In figure 3.5, the experimental setup is shown.

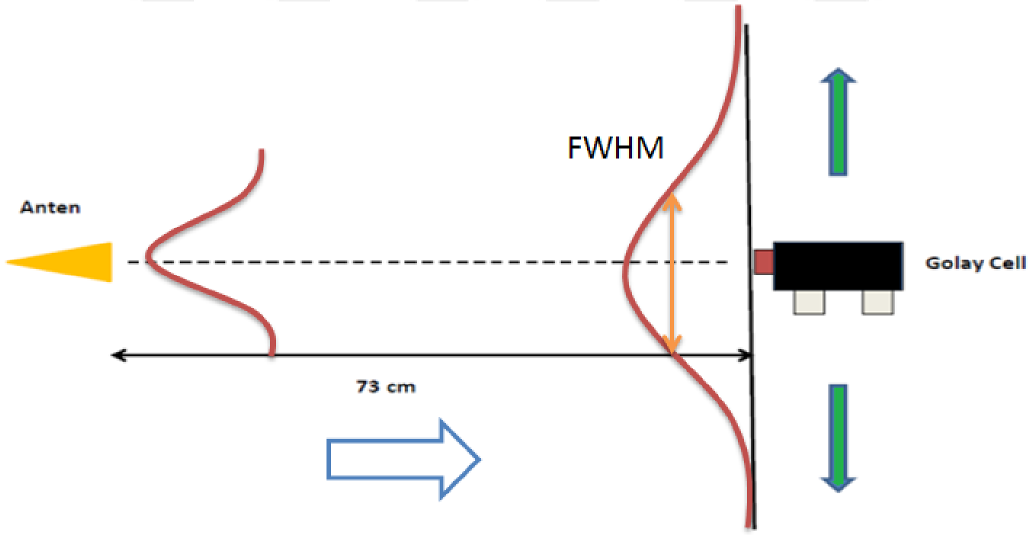

Figure 3.5: Beam power and the beam profile measurement setup

The source runs with TTL modulation with 20Hz repetition rate. Golay Cell was connected to the oscilloscope to observe the oscillation of the power with the modulated frequency. The beam coming from the antenna was characterized by this measurement.During the measurement, Golay Cell was perpendicularly shifted from the optical center of the setup which is shown by dashed lines. In order to increase the resolution of the measurement and the sensitivity of the

Golay Cell, the window of the detector having diameter 11mm was covered by the aluminum sheet. The sheet contains a small pupil having 2mm diameter. Minimizing the window of the detector, full width at half maximum (FWHM) point was determined more precisely. FWHM point gives the divergence angle of the beam from the antenna. In this thesis, the horn has the $(+/-)5.1$ degree half angle [28].

In figure 3.6, the measured data was fit to the function by the scientific software (origin8.1).

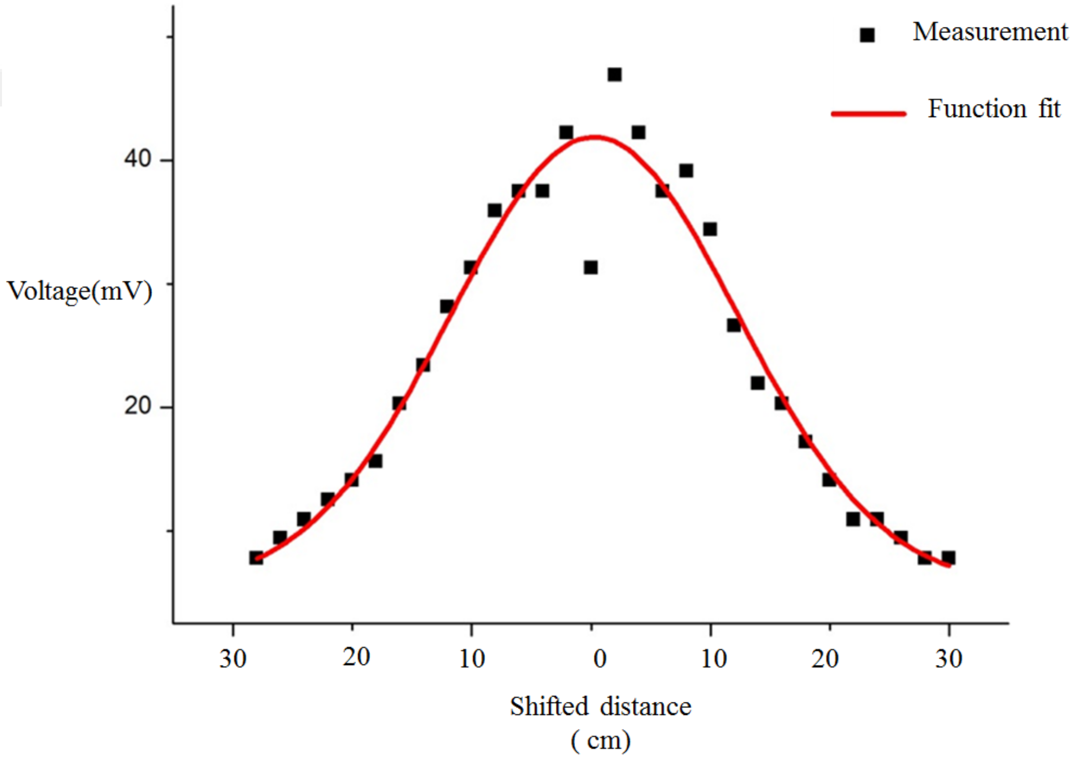

Figure 3.6: The power measurement and function fit

The detector was placed 73cm away from the source and the collected data was correctly fitted by Gaussian function in origin8.1. To determine 3dB angle (FWHM), the red curve is used. The total displacement of the Golay Cell in FWHM region is about 14cm. To calculate the angle, the trigonometric relation was applied.

$$2tan^{-1}\Big(\frac{FWHM/2}{DISTANCE}\Big) = Full\ 3dB\ angle \tag{3.2}$$

By applying the equation 3.2, the full $3dB$ angle was founded 10 degree. This result verifies the horn specification given by the company VDI[28].

In figure 3.6, the maximum power at the center is not stable. Therefore, a second measurement was made without using aluminum foil covering the detector window. At the optical center of the measurement setup, the Gaussian beam intensity distribution is almost flat at $73cm$ away from the source. Therefore,integrating the intensity over the full aperture of the Golay Cell window area gives a stable voltage value, which is measured $581mV$. In order to obtain the output power of the source, the responsivity graph of the Golay Cell, in figure 2.5, was used to convert the voltage to the corresponding power. Equation 3.3 shows responsivity of the Golay Cell depended on the measured voltage value and the power coupled to the window.

$$Responsivity = \frac{the\ measured\ voltage\ value\ of\ Golay\ Cell}{the\ power\ coupled\ to\ thewindow\ of\ Golay\ Cell} \tag{3.3}$$

The gaussian intensity profile which was proven by the measurement is described by the equation 3.4.

$$I = \frac{P_0}{2\pi\sigma^2}e^{-\frac{x^2+y^2}{2\sigma^2}} = \frac{P_0}{2\pi\sigma^2}e^{-\frac{r^2}{2\sigma^2}} \tag{3.4}$$

It is a two dimensional Gaussian distribution equation. P_0 value is corresponding to the output power of the source and small letter "r" effective aperture radius of the detector. The sigma "σ" is standard deviation which is equal to $FWHM/2.35$. The signal power, which was coupled to Golay Cell aperture having $11mm$ diameter, was obtained by the integration of equation 3.5 over a surface integral.

$$P_G = \frac{1}{2}\frac{P_0}{2\pi\sigma^2}\int_0^{2\pi}\int_0^{r} e^{-\frac{r^2}{2\sigma^2}} r dr d\theta \tag{3.5}$$

The scale factor $\frac{1}{2}$ in front of the integral comes from TTL modulation of the source. The result of the integration is shown equation 3.6.

$$P_G = \frac{P_0}{4}\frac{r^2}{\sigma^2} = 2.1x10^{-3}P_0 \tag{3.6}$$

From this result, the output power of $340GHz$ source was approximately calculated $7mW$.

3.4 DYNAMIC RANGE AND LEAKAGE CANCELLATION

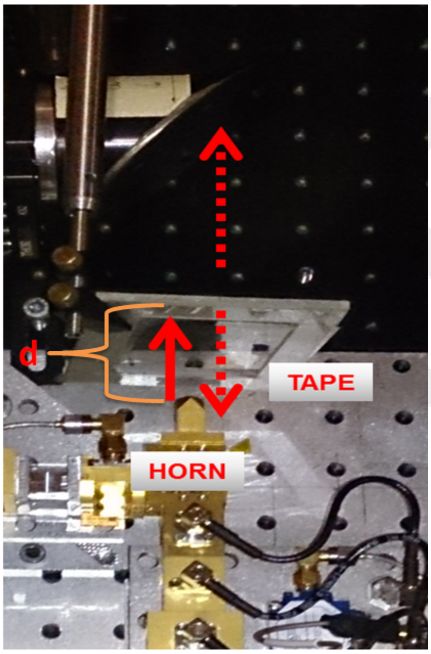

Figure 3.7: The leakage cancellation by placing the tape in front of the horn

In CW operation which will be discussed in chapter 4, the scanning system suffers from the leakage signal coming from the transmitter (T_x) to the receiver (R_x). Initially, it was observed that $-18dBm$ constant leakage is coupled to R_x and this restricts the dynamic range at $13dB$. During the scanning, the returning signal coming from the different points of the target create the varying optical paths. Changing the optical paths of the returning signal causes the interference with leakage signal. This leads to the power fluctuation of the received signal between

$-5dBm$ to $-35dBm$. To solve this problem, a transparent tape was placed in front of the Horn. The tape reflects the small amount of the transmitted signal to the horn again. The leakage and the reflected signal have the same frequency but different phases. By changing the distance "d", the phase difference of two signals was set to π. The phase difference of π between these signals created the destructive interference. It is shown in figure 3.7. After the destructive interference with partially reflecting tape, the leakage signal was reduced to $-25dBm$ and the dynamic range was increased to $20dB$ in CW operation.

3.5 THE FREQUENCY MEASUREMENT

So for, the beam profile, IF signal and the output power of 340GHz source have been measured. However, these measurements do not give the information about the output frequency or wavelength of the source. In laboratory, the best frequency detector is the Marconi 2383 spectrum analyzer and it is limited to 30GHz. Therefore, the new alternative ways were searched. The literature search showed that the metal surfaces having cuttedhole patterns in array structures behaves like a band pass filter[29]. It is called dichroic filter or qasi-optical filters. The filter consists of the holes placed in certain geometry and this structure behaves like a circular waveguide with a cutoff frequency defined by the parameters. These are the dimensions of the holes, the separation of the holes and the length of the waveguide. In figure 3.8, the circular waveguide with its' parameters is represented.

The mathematical calculation of the filter is presented by Chen[29, 30]. Chen combined these parameters into the transmission and the reflection equations of the electromagnetic wave.

$$R = \frac{1}{1 - i[A + Btanh(\beta l)]} + \frac{1}{1 - i[A + Bcoth(\beta l)]} - 1 \tag{3.7}$$

$$T = \frac{1}{1 - i[A + Btanh(\beta l)]} - \frac{1}{1 - i[A + Bcoth(\beta l)]} \tag{3.8}$$

The equations show the complex conjugate components of the transmission and the reflection parameters. The constants A and B differ from the geometry. The

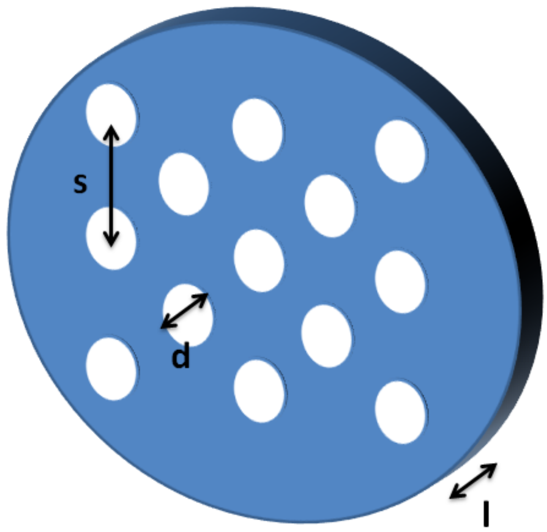

Figure 3.8: Dimensions of the circular waveguide with l is the thickness,d is the diameter of the holes and s is the separation of the holes

filter designed in laboratory has circular holes with triangular placement and the parameters are defined in equation 3.9 and 3.10.

$$A = 12\left(\left(\frac{4}{3}\right)\left(\frac{\lambda}{s}\right)^2 - 1\right)\right)^{1/2}\left[\frac{J_1^1\left(\frac{2\pi d}{\sqrt{3}s}\right)}{1-\left(\frac{2\pi d}{1.841\sqrt{3}s}\right)^2}\right]^2 - \frac{12}{\left(\frac{4}{3}\right)\left(\frac{\lambda}{s}\right)^2 - 1)\right)^{1/2}}\left[\frac{J_1\left(\frac{2\pi d}{\sqrt{3}s}\right)}{\left(\frac{2\pi d}{\sqrt{3}s}\right)^2}\right]^2 \tag{3.9}$$

$$B = 1.32\left(\frac{s}{d}\right)^2\left(\left(\frac{0.586\lambda}{d}\right)^2 - 1\right)^{1/2} \tag{3.10}$$

According to the equations 3.7 and 3.8, the reflected and the transmitted powers are calculated by the modulus square of equations.

$$T_p = |T|^2 \tag{3.11}$$

$$R_p = |R|^2 \tag{3.12}$$

In order to determine the filter parameters, the simulation based on the equations given above was made. In simulation, the filter was designed %100 percent transmission at $340GHz$. The design parameters of the filters are l=50μm,

d=571μm and s=793μm. With the collaboration of Fiberlast company, the filter was fabricated by the pulse laser (NanoMark 20W) having 0.5mJ pulse energy and 25kW beak power with 40kHz repletion rate.The closer view of the filters is shown in figure 3.9.

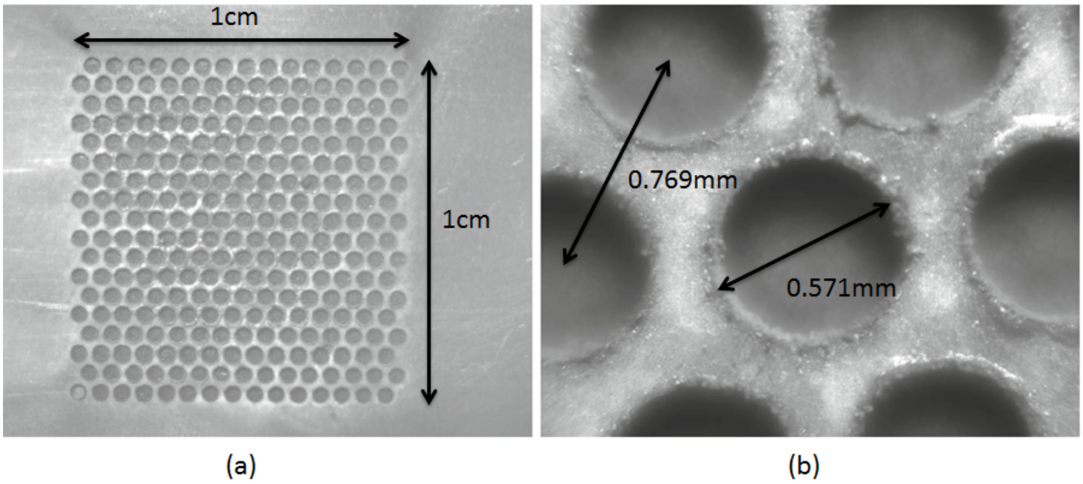

Figure 3.9: (a) The manufactured filter (b) the closer look of the filter [31]

In order to characterize the fabricated filter, THz-TDS system was used in laboratory. The system scans the wide range of THz region between 0.2THz and 2THz. The time domain transmission pulse measurement and the Fourier transform of the pulse shape were compared to the simulation results.

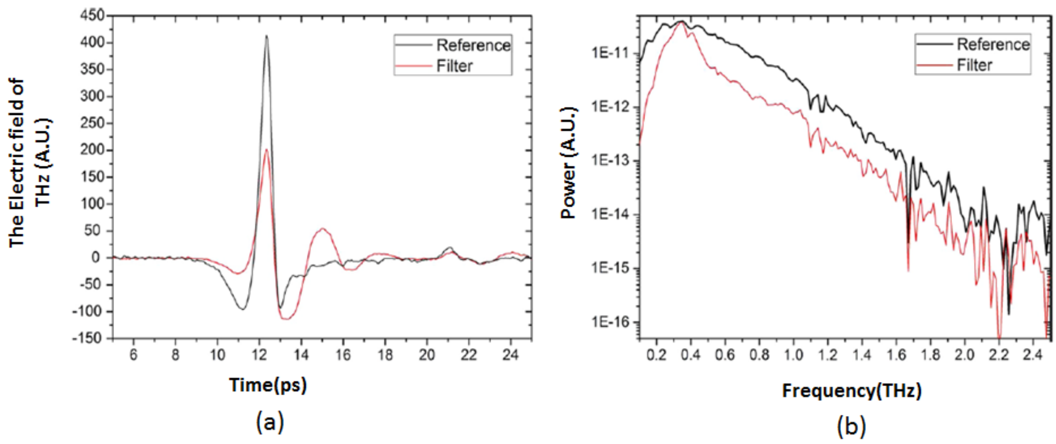

Figure 3.10: (a) Power measurement in time domain (b) power measurement in frequency domain [31]

In figure 3.10, the power measurements of the reference and the filter were compared. The reference measurement is required for the normalization. It is the free space measurement and the transmission power of the free space is shown in figure 3.10(b). The filter has band pass characteristic. In other words, it blocks the partial region of the spectrum. The response of the filter was found by the Fourier domain analysis. In a system, the filter or the response is represented by $h(t)$ in time or $H(f)$ in frequency domain. The signal and the outcome are shown by $x(t)$, $y(t)$ in time and $X(f)$, $Y(f)$ in frequency. In spectroscopy, T-ray is convolved by filter (equation 3.13). In frequency domain (equation 3.14), the convolution in time domain is equal to the multiplication of the filter response and the resulted signal.

$$x(t) * h(t) = y(t) \tag{3.13}$$

$$X(f)H(f) = Y(f) \tag{3.14}$$

The unknown parameter of this equation is the response of the filter ($H(f)$). To find the response of the filter, $Y(f)$ was divided by the reference measurement ($X(f)$) in equation 3.15.

$$H(f) = \frac{Y(f)}{X(f)} \tag{3.15}$$

After the calculation, the simulated and measurement results are compared in figure3.11.

The measurement result, having $30GHz$ resolution, is consistent with the simulation, so this filter was successfully characterized.

The next measurement was made on $340GHz$ source in order to find the output wavelength. The filter was placed between the Golay Cell and $340GHz$ source. The recorded voltage with filter was $770mV$ and without the filter was $850mV$. The measurement shows that the filter has %90 percentage transmission in this wavelength. The estimated frequency of the source was found in between 320GHz and 350GHz. To find the exact frequency, a high cost vector

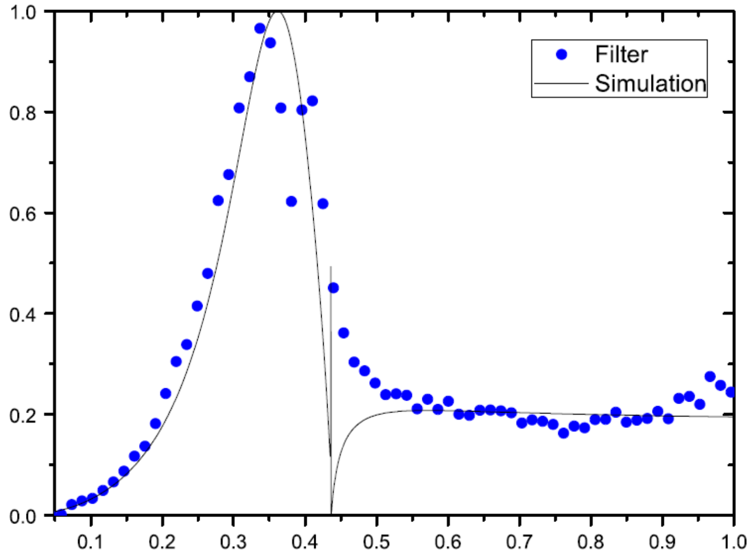

Figure 3.11: The filter measurement compared with simulation [31]

network analyzer (VNA) having operation wavelength $350GHz$ is needed. However, it is not available in our laboratory. Therefore, the frequency measurement was concluded by using dichroic filter in order to determine the wavelength of the source.

3.6 RADAR PULSE MEASUREMENT

The $340GHz$ active imaging system contains optical components in order to focus the beam on the target. The finalized system was designed in compact form. All of the components was placed $1m^2$ area on a platform surface. Therefore, it is a possibility that the back reflections of the beam can be coupled to the source again in CW mode. Therefore, the coupling of the back reflections causes extra noise. To overcome reflections, the system was tested in pulse modulation.

In figure 3.12, the desired operating intervals of the transmitter and the receiver parts are shown. For the target placed in 5 meter away, the total measurement time is planned about $50ns$. T_x and R_x parts were operated in switching mode. The operating time of the T_x and R_x parts are shown in figure 3.12.

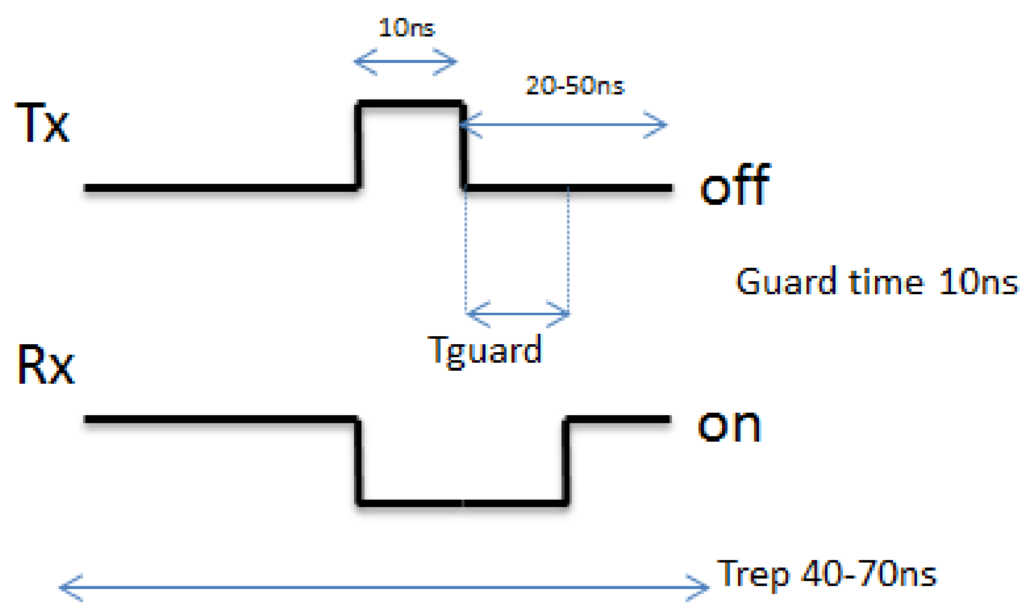

Figure 3.12: Operating intervals of R_x and T_x

In order to prevent the back reflection of the optical components into horn during transmission of the pulse, 10ns guard time will be set. After the guard time, the receiver will be turned on and the incoming signal will be coupled into the horn.

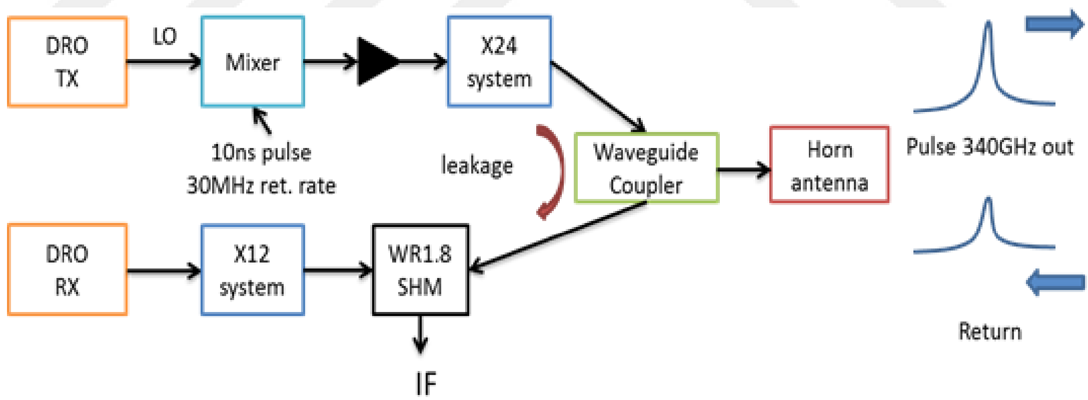

Figure 3.13: The pulse measurement design of the system

In figure 3.13, the modulation design of the source was shown. It is seen that a leakage signal coming from the transmitter can be coupled to the receiver. However, with the proper switching time interval the leakage can be eliminated.

In the experimental setup, a flat metal plate is placed $68cm$ away from the source. In figure 3.14, the measurement setup is shown.

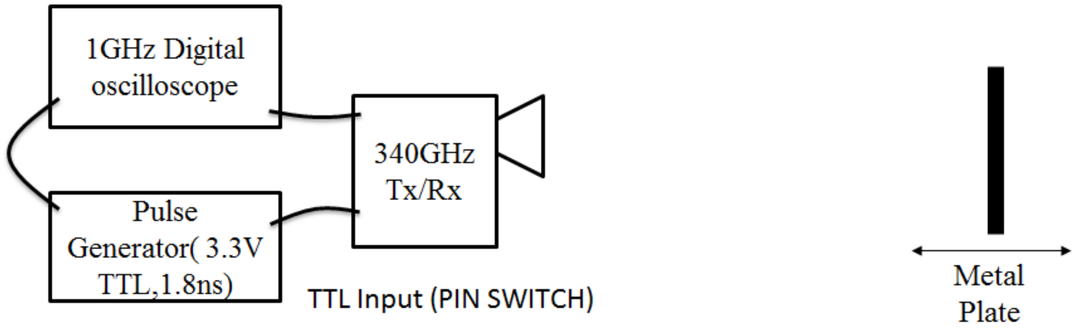

Figure 3.14: The pulse measurement setup

The pulse generator generates pulse in TTL modulation with $1.8ns$ time intervals. During the time interval, the pulse travels $0.54m$ in space. While making the measurement, the receiver was turned on in order to observe the leakage pulse. In order to detect the returning signal from the target, the target should be placed the position where the total traveling time of pulse is greater than the pulse duration. Otherwise, the received signal will overlap with the leakage pulse and no detection will be observed.

In figure 3.15, the measurement results are illustrated. The first peak of the figures is the leakage pulse coming from the directional coupler and the second one is coming from the target plate. First of all, the time difference of the two pulses was about $3.5ns$ which is equal to the one round trip of the pulse and the measured distance is about $56cm$. After the target was shifted a few centimeters away from the source, the time difference of the pulse was measured $3.6ns$. In final measurement, $4.2ns$ time difference from the target is recorded. This corresponds to $68cm$ measured by meter.

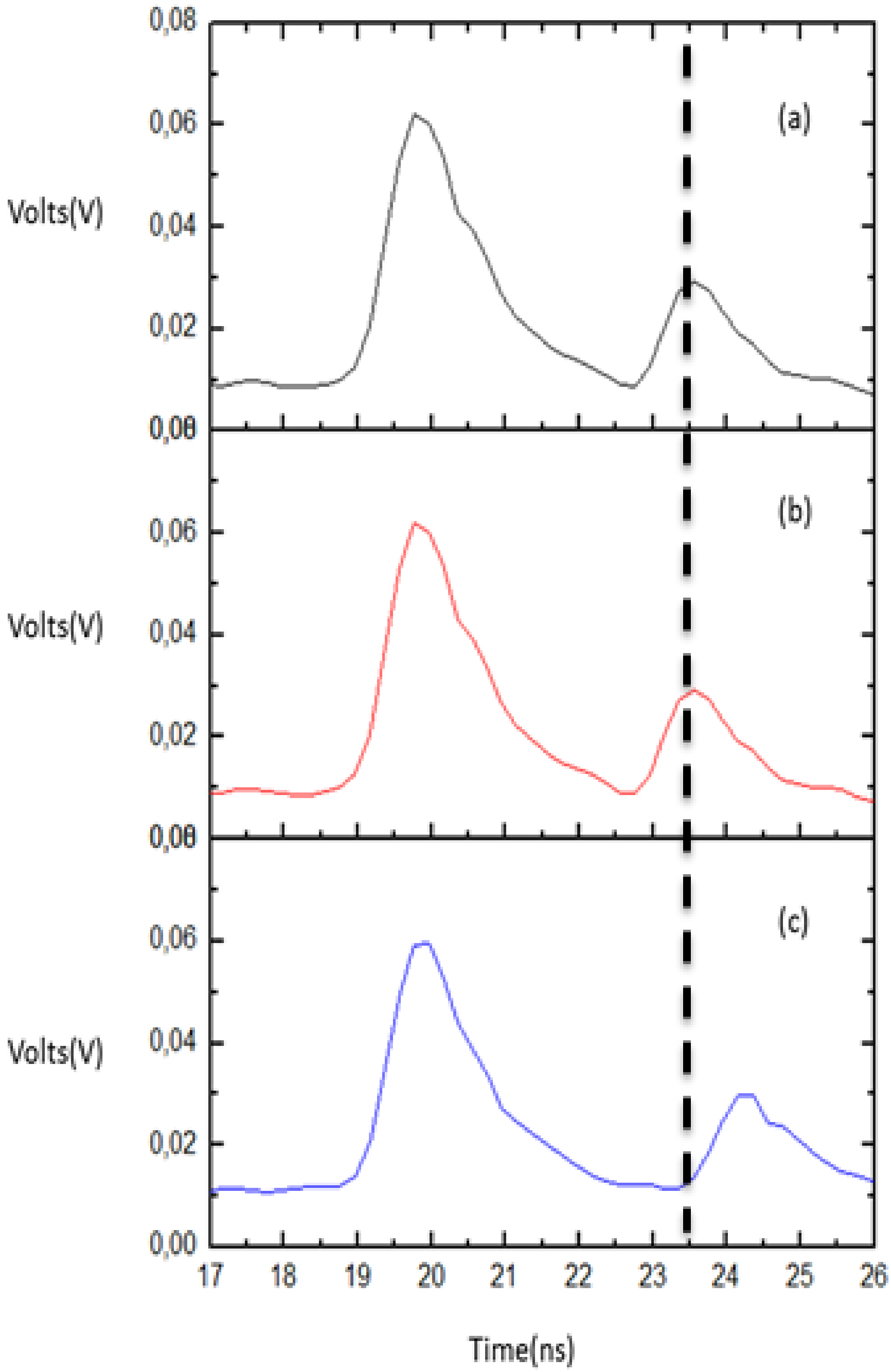

Figure 3.15: The pulse measurement results from the target. The target distances from the source are (a)56cm, (b)58cm and (c)68cm. The dashed line shows the relative position of the first peak with respect to the other peaks.

CHAPTER 4

THz IMAGING SYSTEM

4.1 MIRROR GALVANOMETER SCANNING

In this thesis, the transceiver system will act like a single pixel detector. Without the array detectors, obtaining an image with a single pixel can be only achieved by focusing the beam on the different points of the target. To do so, the galvanometer mirrors were used. For testing the mirrors before integrating them to the main setup, the pre-work scanning system was constructed which will be explained in section 4.3. Both pre-work and the main setup used the same galvanometer mirrors with the same specification. The reason for applying the same specification is that the first system is the pre work of the main setup. The system is designed to scan human body as much as possible. The goal of this project is to perform scanning in 2 $frames/s$ with 30x30 pixels image resolution. It is quite fast as compared to the other THz imaging systems which take minutes to complete scanning.

For the scanning, the data is collected by DAQ (NI USB 6212 BNC 16bit and 250Ksamp/s) is used. In figure 4.1, the block diagram of data collection setup is shown. The beam propagates into the optics and it is focused on the target. The incoming beam reflected from the target is coupled to the transceiver source again and the obtained IF signal converted to DC signal by DAQ card. The two analog outputs are connected to Galvo mirrors and these outputs generates the necessary voltages in order to rotate the mirrors with a given periodic voltage function such as sine, triangular or saw-tooth. The scanning area is set to be

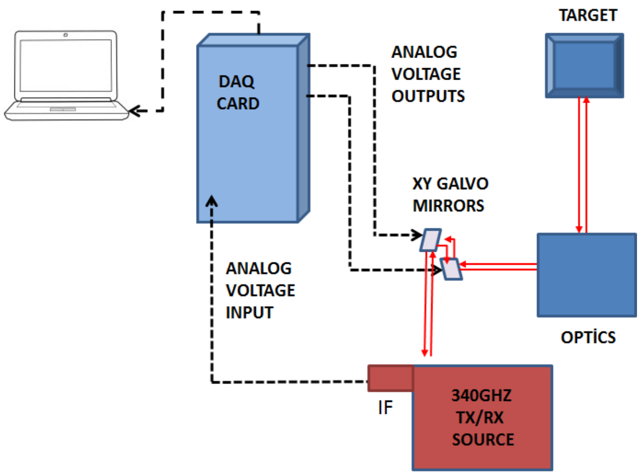

Figure 4.1: The electronic connections of the scanning system

square shaped and having 30x30 pixels resolution in 2 $frames/s$. To achieve this goal X mirrors horizontally vibrates in $30Hz$ and the Y mirror vertically vibrates in $1Hz$. In figure 4.2, the raster scanning on the target is illustrated.

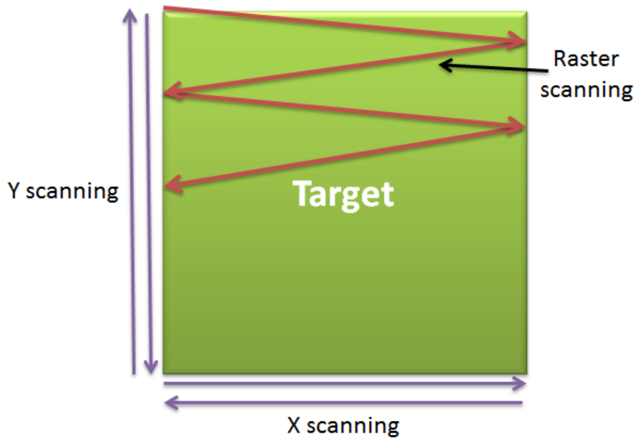

Figure 4.2: The raster scanning and the position of the mirrors

The applied voltage on the mirrors is set to be triangular shapes. The reason for this is the simplicity of the reconstruction of the image. The scanning speed is the same for all points on the target. Therefore, any unnecessary differential calculation is avoided during the reconstruction algorithm of the image.

During the scanning of the mirrors, DC power coming from IF signal is digitized in DAQ. One scan is completed in $0.5s$ and it is converted to the image. The sampling rate of this system is set to 18000 *samples/s*. The image resolution mentioned above is 30x30 pixels. It contains 900 pixels in each frame. The system collects 10 data points for each single pixel. The sampling rate which requires to image reconstruction is 10 times higher than the total number of pixels. It means that the data collected from each pixel is oversampled. 10 data points for each pixel are summed and the average value of this summation is displayed on the screen as a measured value of the pixel. In the next sections, the images taken from this scanning system will be discussed more clearly with a given measurement examples.

4.2 POINT SPREAD FUNCTION (PSF) AND MODULATION TRANSFER FUNCTION (MTF)

PSF is the tool to measure the response of an image coming of the point source. It is a wave dependent function. PSF is the special domain function of the optical transfer function (OTF). The Fourier transform of OTF is corresponding to the PSF function. The PSF function can be used for the simulation of the spots on the target[32]. The real part of the complex OTF function is known as MTF. MTF is a 2D graph and is used for determining the resolution of the optical system. The resolution of the system is calculated by MTF graph. The value stated at %50 percent of MTF graph is taken the inverse half of it, which will give the minimum separation distance between two points. The calculation of the resolution from MTF will be shown in sections 4.3 and 4.5 for different optical setups.

4.3 THE FIRST SCANNING SYSTEM IN 340GHz SETUP

In spring 2014, the first 340GHz standoff active imaging of our system was performed. The directional coupler, connecting transmitter and receiver to each other, causes the leakage flow in CW mode. This results in limiting the dynamic range of the system. In section 3.5, the leakage cancelation solution and detailed explanations have been given.

In this pre-work, the block diagram of the first standoff active imaging system is shown in figure 4.3 [33] .In figure 4.4, the orange lines show the ray tracing in this setup. Beam emitted from the antenna is focused on the image plane where the target is placed.

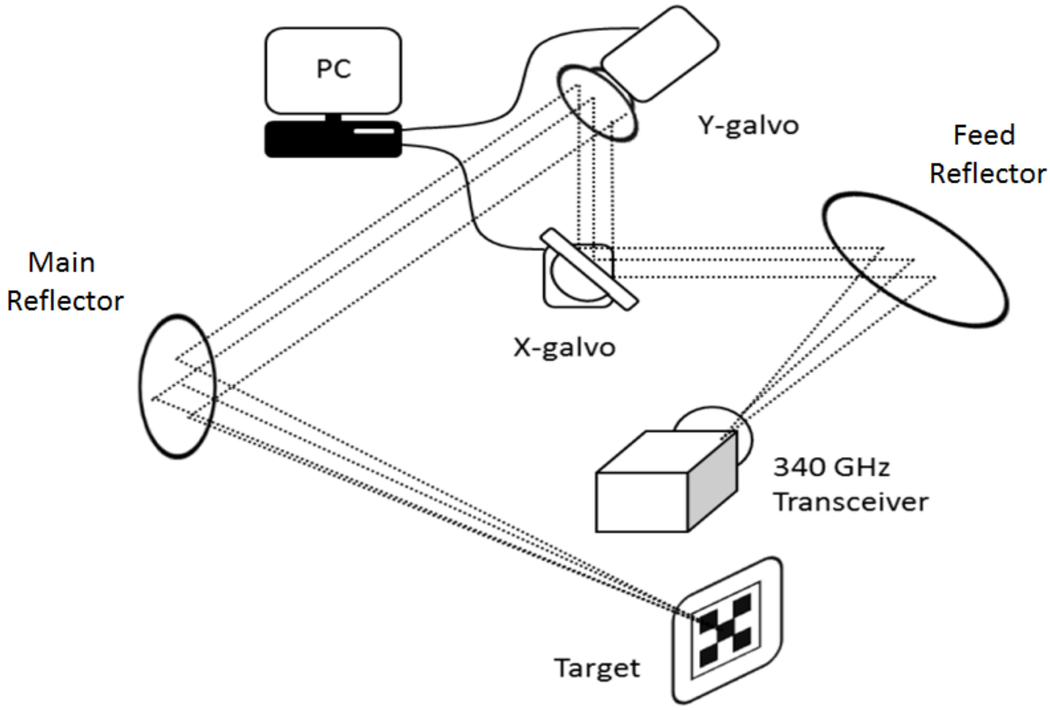

Figure 4.3: The first imaging setup of 340 GHz source

The beam radiates from the source antenna and the source was placed on the focal point of the first parabola. The parabola ($F\#1.8$, $D = 63.5mm$) having 90 degrees off-axis collimates the beam.The next mirrors, made of beryllium, are XY scanning galvanometric mirror assembly (Crisel Instruments G4080). These mirrors perform 2D scanning. In order to focus the scanned spots on the target, a second 30 degree off-axis parabolic mirror ($F\#3$, $D = 101.6mm$) was used. In figure 4.5, the target which had been used is made of aluminum and having square holes. It has $4cm$ x $4cm$ dimensions and $0.2mm$ thickness. In order to fabricate this aluminum pattern with high precision and without any defects on patterns, a pulsed laser had been used. It has $40kHz$ repetition rate, $0.5mJ$ average pulse energy with 25kW peak power per pulse.

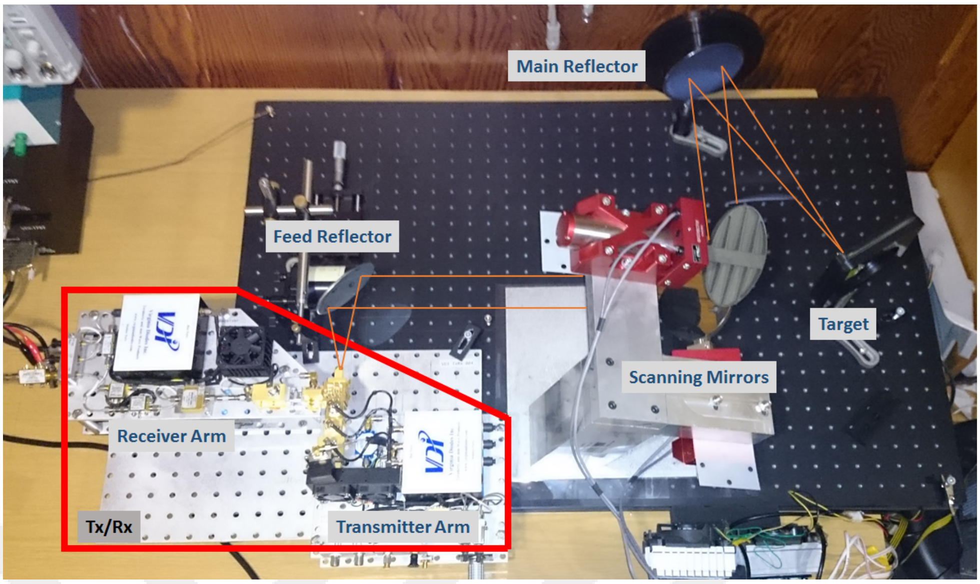

Figure 4.4: The picture of the first imaging setup

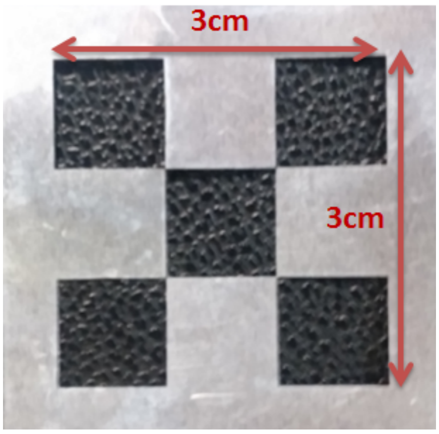

Figure 4.5: The target of the scanning system [33]

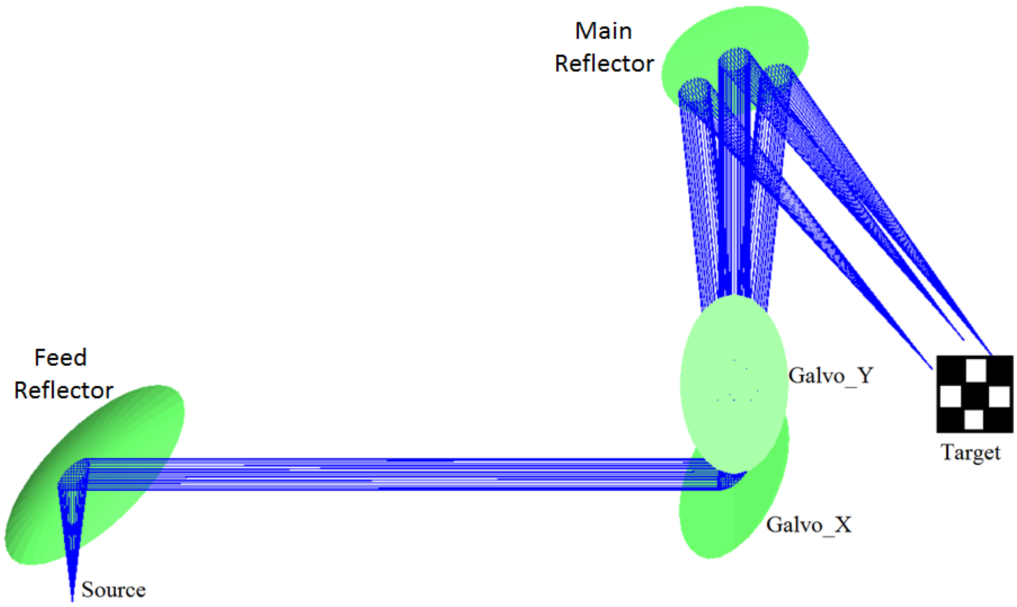

Figure 4.6: The ray tracing of the beam optical system [33]

In figure 4.6, during the X-Y scanning, the positons of the spot on the target are shown. The total optical path from the source to target is 120mm.

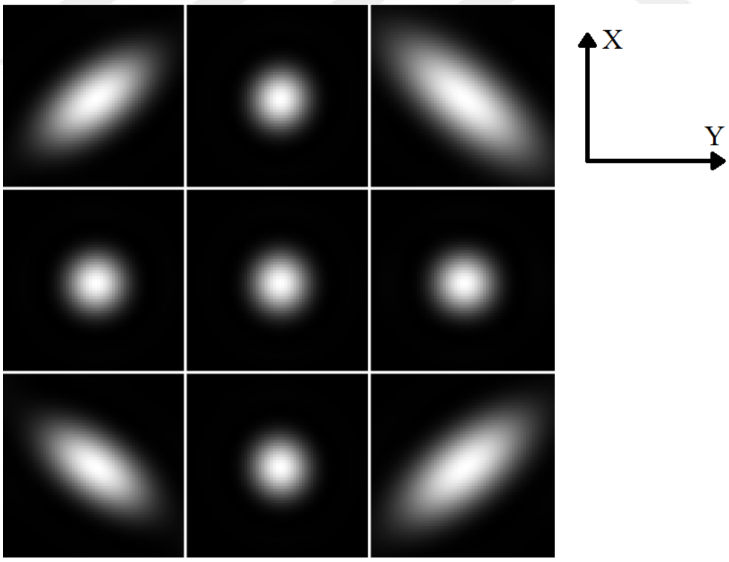

Figure 4.7: The image of PSFs on the target plane [33]

To simulate the spot size of the target, the Gaussian beam propagation analysis have been used and the spot size on the target was founded around 1cm diameter. In figure 4.7, the simulated spot diagram are shown.

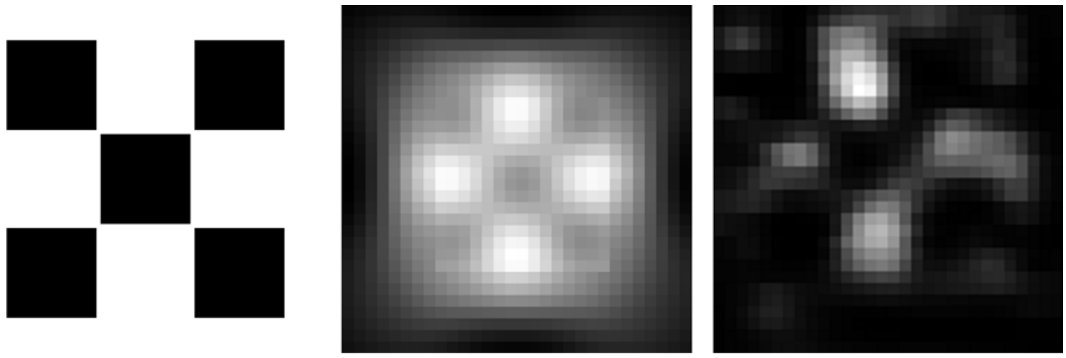

Figure 4.8: (a) The ideal object. (b) PSF given in figure 4 applied on ideal image. (c) the scanning results of the image [33]

By applying PSFs on the image, the ideal image was reconstructed in the simulation program and compared with the measured image of the target in figure 4.8.

4.4 CONFOCAL GREGORIAN GEOMETRY

The main optical platform for the standoff active imaging is based on Confocal Gregorian Geometry. In principle, this geometry performs its scanning application by using elliptical main reflector having two focuses, a sub parabolic reflector and a scanning mirror. In figure 4.9, the position of the mirrors is shown.

The beam is emitted from antenna with a radiation angle θ_f and a feed reflector (parabola) makes the beam collimated. After the collimated beam reflects from the scanning mirror having a rotation capability in 2D (x,y), the beam refocus on the focal point of the sub reflector(parabola) F_s. It is a common focus point for both the ellipsoidal main reflector and the sub reflector. Geometrically, an ellipse has two focal points. The beam coming from the near focal point of the main reflector F_m is refocused on the far focal point which is on the image plane of the optical system [11, 34].

This geometrical design has some benefits on the imaging systems. First of all, the main aperture is stable because the inertia of the main reflector is very

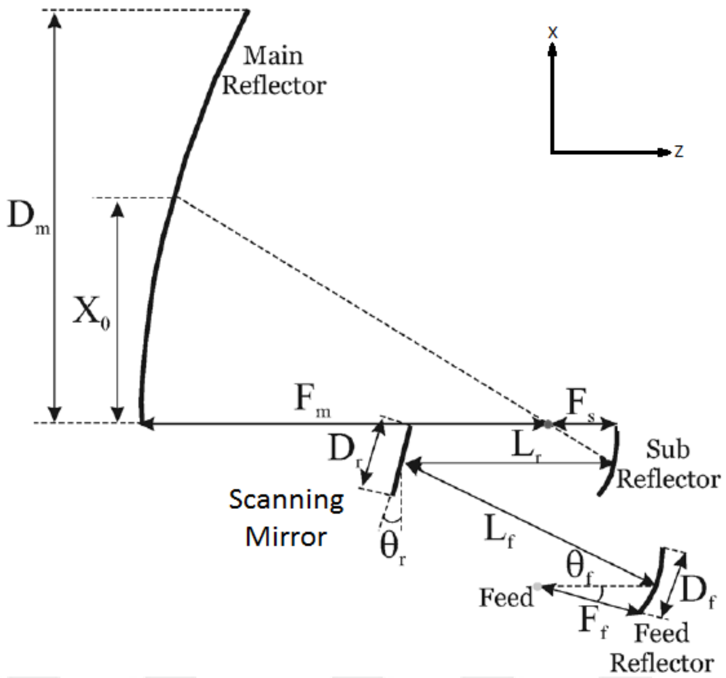

Figure 4.9: The Confocal Gregorian Geometry [11]

large and it is hard to rotate the main reflector. Instead of rotating the main reflector, the rotation is made by flat scanning mirrors having small inertia for a rapid scanning motion. The second benefit is that all of the electrical and the optical components remain stable in design and this provides some simplicities during tests and the characterization of the system such as back reflections, phase shifting of the signal. Finally, the collimating and the refocusing of the beam by using the paraboloid reflectors rather than it goes to the main reflector directly, cause the negligible aberrations over the large field of view [7].

4.5 OPTICAL DESIGN OF THE MAIN SYSTEM

In this part, the optical system design and its performance will be explained. The reference geometry of this system is Confocal Gregorian Geometry which is described in section 4.4. The optical system was designed for the target placed 5 meter away from the main reflector. FOV of system is $0.5m$ x $0.5m$. Optical software was used for designing and optimization stages. In figure 4.10, the software output of the design is shown.

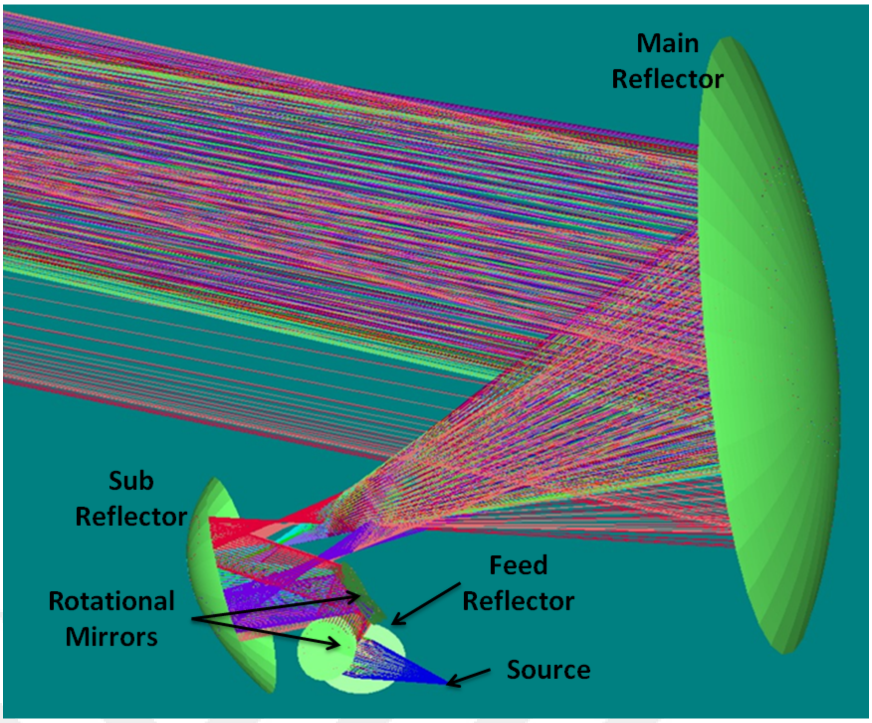

Figure 4.10: Optical design of the main system

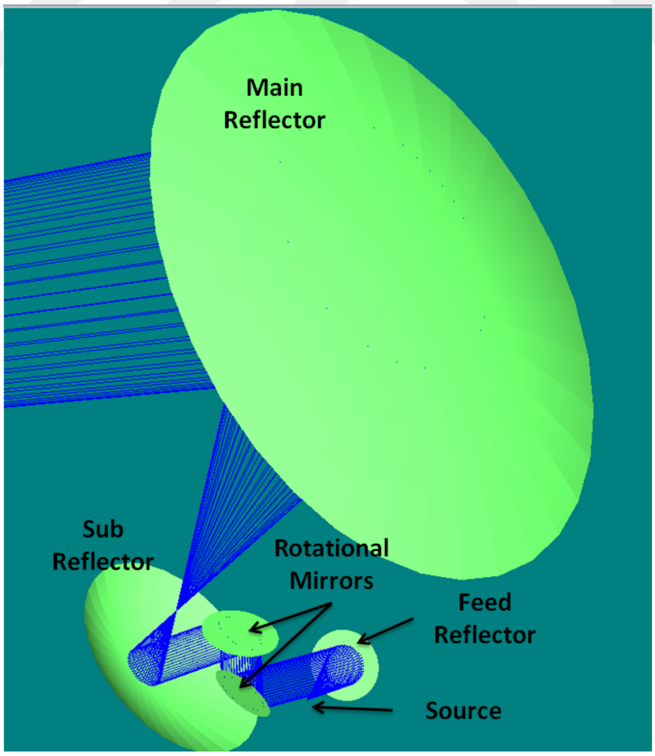

Figure 4.11: Optical design with central ray

It is shown in figure 4.10, the light coming from the source point is reflected from the feed reflector (parabola), which collimates the beam, and then it goes rotational mirrors. Due to the angle of view, the collimated beam does not be seen well. In figure 4.11, the optical path of the central beam is shown clearly.

Each of the rotational mirrors rotates 8 degree half angle in order to scan FOV area. The colourful rays represent the scanning beam having different angle of rotation and being focused on the different points on the image plane. After the reflection of the collimated beam from the rotational mirrors, it reflects from the sub-reflector and focuses on the common focal point of the sub reflector and main reflector. The ellipsoidal main reflector refocuses the beam on the far focus if the beam is coming from the near focus.

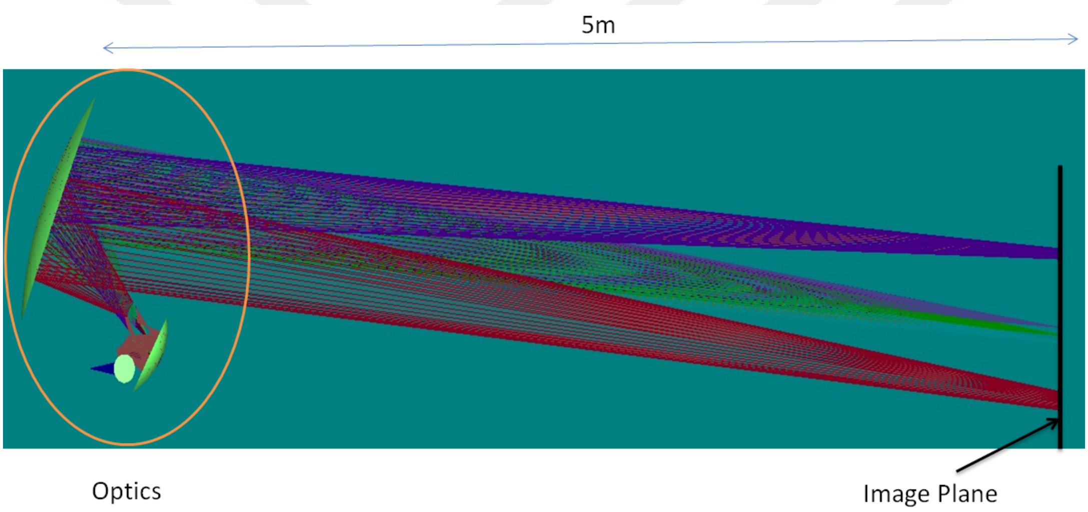

Figure 4.12: The ray patterns on the image plane

In figure 4.12, the image plane is placed at the far focus of the main reflector. The resolution of the system differs from each point on the image plane. The system was optimized by MTF in order to achieve the best spot size at the center of the image plane or FOV.

In figure 4.13, the final configuration of the optical system platform is shown. An extra flat mirror was placed in front of the $340GHz$ source in order to change the direction of the beam. In figures 4.10 and 4.11, the beam directly goes to the feed reflector. However, the holder of Galvo mirrors intersects with the $340GHz$

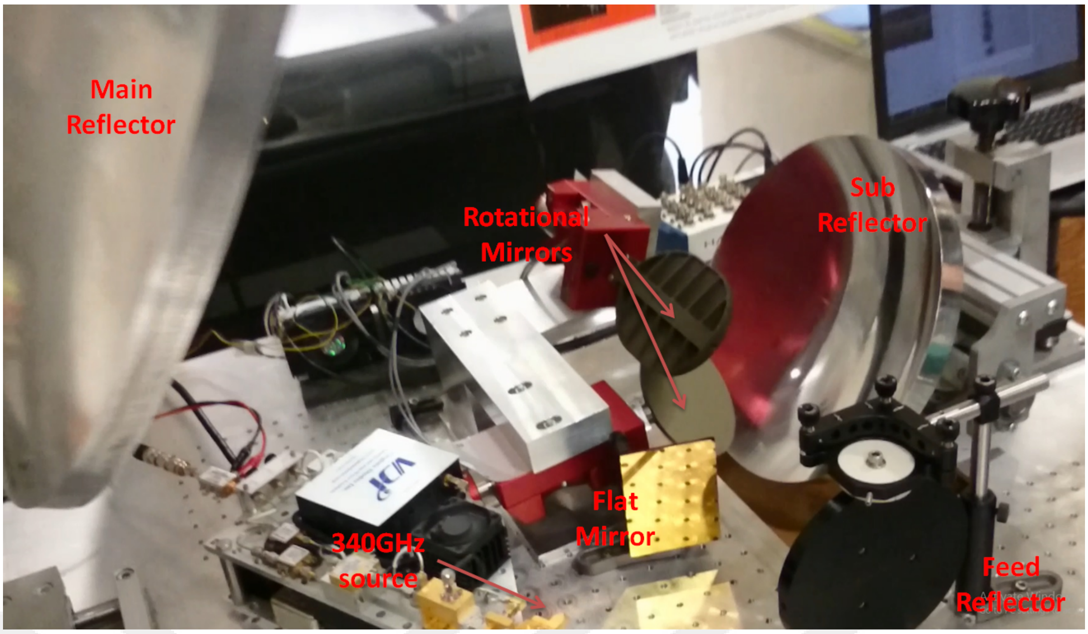

Figure 4.13: The image of the optical platform

source. Therefore, mechanically it was a necessary modification to add an extra flat mirror in order to change the position of the source without changing the optical path.

By using Huygens principle of the software, the PSF functions of 9 discrete points of FOV at $5m$ away were obtained. In figure 4.14, the PSFs are shown. It can be seen that the PSF has the best shape at the center, which means that optical aberrations are minimized. At the edges, the coma and the astigmatism are observed. The coma occurs due to the off-axis of the optical system. The reason of the astigmatism is different radius of curvatures of the main reflector on the horizontal and the vertical dimensions.

Determining the minimum pixel sizes and the resolution of the system, the Huygens MTF which is calculated at the center of the FOV was used. There are two solid lines on the MTF curve and they overlap. It means that the MTF curve is symmetric in 2 dimensions. The same outcome is observed on PSF distribution at the center, shown in figure 4.14. The cycles per millimeter at the 50 percent of the MTF graph was found 0.0340. The inverse of this number gives the minimum separation of two lines in order to distinguish them from each

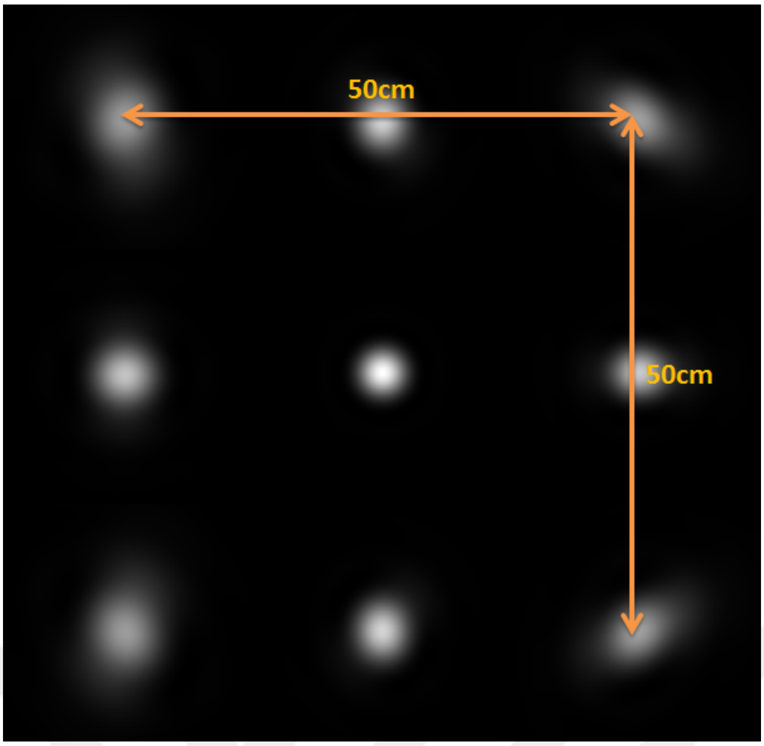

Figure 4.14: The PFS distributions of 340GHz system in 0.5m x 0.5m FOV

other. The half of separation is described as the resolution at the given point. At the center, the system has the best resolution, $1mm/(2*0.034) = 14.7mm$. According to this result, the maximum number of pixels of the imaging system in 0.5m x 0.5m FOV is corresponding to 30x30pixels. It is obtained that the system has 14.7mm spot resolution with 30x30pixels image resolution.

4.6 SCANNING RESULTS OF THE SYSTEM

The scanning of an object was made after finishing the optical alignment. The result of scanning system matches with the design specifications. A flat metal stick, having 3cm thickness and reflection coefficient 1, was placed at the image plane of the system and it caused the specular reflection. So far, three measurements have been made. The first one is the reference measurement without any obstacles in front of the image. The second measurement shows that the scanning is the orientation sensitive. The last measurement was made with an obstacle, polar fleece.

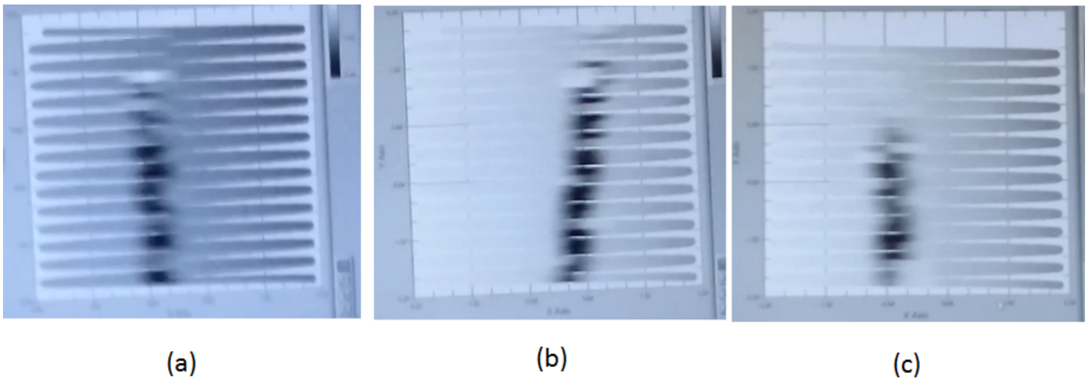

Figure 4.15: (a) The reference measurement, (b) tilted object, (c) object behind the dress

In figure 4.15, the raw data of the $340GHz$ measurements are shown. The scanning positions and the data collected from the current mirror positions were displayed on the screen. To improve the illumination of the pixels, the data collected from the image plane is normalized in each frame. The reconstruction algorithms in video rate have not studied yet in this thesis. To calculate the received power from the object, the equation 1.3 is used below.

$$P_r = A_r\Big(\frac{P_t}{\Theta(2D)^2}\Big)e^{-2\alpha_b L_b}e^{-2\alpha_a D}e^{-2\alpha_e L_e}$$

The target is placed at the image plane, 5m away, and the cross section area of the receiver A_r is the same as the area in solid angle which is used for calculating the transmission power of the system ($7mW$ or $8.45dBm$). The absorption coefficient of the atmosphere α_a at $340GHz$ is $10^{-3}m^{-1}$. In figure 4.15(a), the received power P_r at a given distance $D = 5m$ was calculated at $1.7mW(2.3dBm)$.

In figure 4.15(b), the stick was tilted on the image plane and the object was detected in FOV again. In figure 4.15(c), a black dress was used as barrier in front of the metal stick. The transmission fraction of the black dress at 340GHz is about 0.9, so the decreasing the magnitude of the power with respect to the square of the fraction was found as $1.377mW(1.39dBm)$.

In case of a sphere object on the image plane, the object will scatter the incoming wave with $\Theta/4\pi$. Applying this result to the equation, the returning signal of reference and the measurement with black dress are $-17dBm$ and $-18dBm$.

The result shows that the dynamic range of the system is capable for detecting flat metal surfaces and the measured powers are above to the leakage level for specular reflection. However, detecting the objects causing diffuse reflection is required to improve dynamic range of the system. To do so, the system will be tested with pulse modulation in the future.

CHAPTER 5

CONCLUSION

In this thesis, the main motivation is to detect concealed objects like metals, and plastics from a standoff distance ($5m$) by using an imaging system based on mm wave/THz radiation. A prototype THs standoff active imaging system at $340GHz$ frequency was successfully constructed and tested for the first time in Turkey. While constructing the prototype, the properties of the THz sources, the detection methods of T-rays and designing of an optical system were well studied.

Towards this goal, first the generation and the detection methods for THz radiation were studied. By using frequency up-conversion based on microwave DRO sources, amplifiers and diode multipliers (Schottky) a $340GHz$ transceiver was utilized in the final design of the imaging system. The working principle of the Schottky diode based frequency multipliers and DRO frequency generators were studied and verified throughout the study. A heterodyne detection scheme was employed in the detection of the THz radiation and the principles behind heterodyne and homodyne measurement techniques are discussed.

The output power, output frequency, beam profile and measurement dynamic range of the $340GHz$ transceiver was characterized. By using the Golay Cell, the intensity distribution of the beam profile was found. From the Gaussian shape the divergence of the beam was assessed and the output power of the system was measured to be $7mW$ ($8.45dBm$). The dynamic range of the system initially was about $13dB$ in CW mode due to leakage from the directional coupler specifically designed for the transceiver. To increase the dynamic range of the system, a transparent tape was used and placed at the output of the pyramidal horn. The improved dynamic range was recorded to be about $20dB$.

The transceiver was incorporated in an optical system that was specifically designed for the purpose of the standoff active imaging. The Confocal Gregorian Geometry was used in order to perform scanning with large oscillating mirrors which have low inertia and high rigidity. The final optical design used 6 mirrors, and the main elliptical mirror and secondary parabolic mirror were machined from bulk aluminum. The overall system including the transceiver was constructed to fit in a volume of about $1.5m^3$. The system was placed on a platform which could move up and down, as well as tilt and rotate azimuthally to scan targets as a standoff distance of about $6m$. The resolution of the first prototype system is consistent with the simulation result and was demonstrated to be about $1.5cm$ at the center of the field of view which was measured to be $0.5m$ x $0.5m$, constrained by the scanning angle of the XY-galvonometer mirrors. The received power of the system was calculated by using a transmission equation based on the well known Friis equation[10]. Mainly two cases, which are the received power from the flat surface causing specular reflection and a spherical surface causing diffuse reflection, were studied under two conditions with and without a barrier (heavy jacket). For the specular reflection case, the received powers were $1.7mW$ ($2.3dBm$)) without barrier and $1.377mW$ ($1.39dBm$) with the barrier. In the second case, due to diffuse reflection, the received power reduced to $-17dBm$ without and $-18dBm$ with the barrier. These results remain in the dynamic range of our constructed system making detection possible.

In the future, the dynamic range of the prototype will be increased by pulse modulation in order to detect objects causing less reflection. Moreover, the system will be tested under different weather conditions with different kind of barriers to detect obscured objects. Furthermore, the integration of the optical and electrical components on the platform will be completed. Finally, the weight balance of the components on the platform will be well calculated to prevent any injuries. Development of this system will serve as a basis for the development of longer distance standoff imaging systems.

REFERENCES

[1] Shin'ichiro Hayashi and Kodo Kawase. *Terahertz-wave parametric sources.* Number January. 2010.

[2] Michael C. Kemp. Explosives Detection by Terahertz Spectroscopy—A Bridge Too Far? *IEEE Transactions on Terahertz Science and Technology*, 1(1):282–292, 2011.

[3] Enis Arik, Hakan Altan, and Okan Esenturk. Dielectric properties of ethanol and gasoline mixtures by terahertz spectroscopy and an effective method for determination of ethanol content of gasoline. *Journal of Physical Chemistry A*, 118(9):3081–3089, 2014.

[4] Andriy Danylov. THz laboratory measurements of atmospheric absorption between 6% and 52% relative humidity. *Submillimeter-Wave Technology Laboratory, University of Massachusetts Lowell*, (September):1–7, 2006.

[5] Douglas T. Petkie, Corey Casto, Frank C. De Lucia, Steven R. Murrill, Brian Redman, Richard L. Espinola, Charmaine C. Franck, Eddie L. Jacobs, Steven T. Griffin, Carl E. Halford, Joe Reynolds, Sean O'Brien, and David Tofsted. Active and passive imaging in the THz spectral region: phenomenology, dynamic range, modes, and illumination. *Journal of the Optical Society of America B*, 25(9):1523, 2008.

[6] Yun Shik Lee. *Principles of terahertz science and technology.* 1 edition, 2009.

[7] Nuria Llombart, Robert J. Dengler, and Ken B. Cooper. Terahertz Antenna System for a Near-Video-Rate Radar Imager [Antenna Applications]. *IEEE Antennas and Propagation Magazine*, 52(5):251–259, 2010.

[8] Shung-Wu Lee. *Antenna Handbook: Theory, Applications, and Design 1988*, volume 1. 1 edition, 1988.

[9] E. R. Brown. Fundamentals of terrestrial millimeter-wave and thz remote sensing. *International Journal of High Speed Electronics and Systems*, 13(04):995–1097, 2003.

[10] John F Federici, Brian Schulkin, Feng Huang, Dale Gary, Robert Barat, Filipe Oliveira, and David Zimdars. THz imaging and sensing for security applications—explosives, weapons and drugs. *Semiconductor Science and Technology*, 20(7):S266–S280, 2005.

[11] Nuria Llombart, Ken B Cooper, Robert J Dengler, Tomas Bryllert, and Peter H Siegel. Confocal Ellipsoidal Reflector System for a Mechanically Scanned Active Terahertz Imager. *IEEE Transactions on Antennas and Propagation*, 58(6):1834–1841, 2010.

[12] S. Preu, G. H. Dhler, S. Malzer, L. J. Wang, and A. C. Gossard. Tunable, continuous-wave Terahertz photomixer sources and applications. *Journal of Applied Physics*, 109(6), 2011.

[13] Ho Jin Song, Katsuhiro Ajito, Yoshifumi Muramoto, Atsushi Wakatsuki, Tadao Nagatsuma, and Naoya Kukutsu. Uni-travelling-carrier photodiode module generating 300 GHz power greater than 1 mW. *IEEE Microwave and Wireless Components Letters*, 22(7):363–365, 2012.

[14] R. D. Richtmyer. Dielectric Resonators. *Journal of Applied Physics*, 10(6):391, 1939.

[15] A Petosa and A Ittipiboon. Dielectric Resonator Antennas: A Historical Review and the Current State of the Art. *IEEE Antennas Propag. Mag.*, 52(5):91–116, 2010.

[16] Dongho Kim. Planar Magneto-Dielectric Metasubstrate for Miniaturization of a Microstrip Patch Antenna. *Microwave and Optical Technology Letters*, 54(12):1064–1067, 2012.

[17] T.D. Iveland. Dielectric Resonator Filters for Application in Microwave Integrated Circuits. *IEEE Transactions on Microwave Theory and Techniques*, 19(7):643–652, 1971.

[18] Asamitsu Higasisaka Hideo Takamizawa Hiroyuki Abe Yoichiro Takayama. A Highly Stabilized Low-Noise GaAs FET Integrated Oscillator with a Dielectric Resonator in the C Band. *IEEE Trans. Mictrowave Theory and Techniques*, 26(3):156–162, 1978.

[19] John Everett, Rachel Abbott, and Damien Boyd. *Very Small Aperture Terminals (VSATs) (Telecommunications) Make Money with Us*. 1992.

[20] Charles Kittel. *Introduction to Solid State Physics*. Number 1. 8 edition, 2005.

[21] Ferenc Marki. Mixer Basics Primers. 2010.

[22] M.J.E. Golay. Theoretical consideration in heat and infrared detection, with particular reference to the pneumatic detector. *Review of Scientific Instruments*, 18:347, 1947.

[23] C. R. Boggs. *Characterization of Room Temperature Terahertz Direct Detectors*. PhD thesis, Wright State University, 2010.

[24] David W Ball. Photoacoustic Spectroscopy. *Spectroscopy*, 21(September):14–16, 2006.

[25] Craven and R. R. Thomas. Waveguide antenna switches using p-i-n diodes. *Electron Lett*, 13(24):518–520, 1977.

[26] Virginia Diodes Inc . Waveguide Band Designations, 2010.

[27] Leon W. Couch. *Digital and Analog Communication systems*. Pearson, 8 edition.

[28] Virginia Diodes Ing. Nominal Horn Specificatinos, 1998.

[29] C.C. Chen. Transmission of microwave through perforated flat plates of finite thickness. *IEEE Transactions on Microwave Theory and Techniques*, 21(1):1–6, 1973.

[30] C. Winnewisser, F. Lewen, and H. Helm. Transmission characteristics of dichroic filters measured by THz time-domain spectroscopy. *Applied Physics A: Materials Science & Processing*, 66:593–598, 1998.

[31] Taylan Takan, Hakan Keskin, and Hakan Altan. Low-cost bandpass filter for terahertz applications. *Optical and Quantum Electronics*, 47(4):953–960, 2015.

[32] V. A. Özkan. *Image Reconstruction Based On Active Scan Techniques In The Terahertz Frequency Range*. PhD thesis, Middle East Technical University, 2014.

[33] İhsan Ozan Yıldırım, Vedat a. Özkan, Fırat İdikut, Taylan Takan, Asaf B. Şahin, and Hakan Altan. Image reconstruction and optimization using a terahertz scanned imaging system. 9250:925005, 2014.

[34] Ken B Cooper, Robert J Dengler, Nuria Llombart, Ashit Talukder, Anand V Panangadan, Chris S Peay, Imran Mehdi, and Peter H Siegel. Fast, high-resolution terahertz radar imaging at 25 meters. *Proc. of SPIE, Terahertz Physics, Devices, and Systems*, 7671:76710Y, 2010.